Functional and Structural Characterization of Mesolimbic and Nigrostriatal Networks in Adult ADHD: Identifying Pathological Effects and Therapeutic Targets

Arjun Sethi

Thesis submitted to Brighton & Sussex Medical School

for the degree of Doctorate of Philosophy

June 2016

Abstract

Attention Deficit Hyperactivity Disorder (ADHD) has been widely associated with abnormalities within the dopamine system. However, the nature of these changes, and how they are targeted by medication is unclear. For instance, though childhood ADHD is robustly associated with abnormal striatal morphology in voxel-based morphometry (VBM) studies, these changes are not necessarily observed in adulthood, which has been argued to reflect normalisation with treatment and maturation. However, findings for this hypothesis are inconsistent. Moreover, although dopaminergic signalling driven by the substantia nigra/ventral tegmental area (SN/VTA) is central to most theoretical accounts of ADHD, little research has examined how this structure and its subcomponents contribute to the disorder. Finally, although mesolimbic dopamine system abnormalities have been linked to altered reinforcement learning in ADHD, the mechanisms underpinning this are unclear. Recent advancements in MR and computational methodologies are well positioned to resolve these questions. This thesis employs several such methodological advancements to clarify the role of mesolimbic and nigrostriatal systems in ADHD. Firstly, I show that by using magnetisation transfer (MT) saturation maps optimised for subcortical contrast, striatal volumetric reductions are observed in VBM analyses of adults with ADHD. Moreover, I show that T1-weighted volumes used in previous studies are insensitive to these differences, and that prior assessments may have been confounded by other factors such as altered brain iron concentration. The second line of investigation uses diffusion MRI parcellation methods to provide the first microstructural assessment of SN/VTA subcomponents in ADHD, revealing distinct functional contributions. Specifically, microstructural differences in the nigrostriatal and mesolimbic SN/VTA appear to respectively underpin trait motivation and waiting impulsivity, and also appear to be differentially targeted by long term medication. The final study uses a temporal difference (TD) model to isolate computational parameters of reinforcement learning altered in ADHD. In doing so, this reveals impaired reward learning in ADHD that is ameliorated by stimulant medication, and several mechanisms underpinning this. Namely, stimulant medication appears to improve learning rates and reduce aberrant novelty processing within the SN/VTA in a manner specific to ADHD. Collectively these findings indicate the ongoing relevance of mesolimbic and nigrostriatal systems in adult ADHD. Moreover, this work shows that appropriate application of novel methodologies has the potential to answer previously unresolved questions in the literature, as well as offering a finer-grained understanding of how these systems contribute to the disorder.

Contents

Acronyms and Definitions

ADHD – Attention Deficit Hyperactivity Disorder

BDI – Becks Depression Inventory

CAARS – Connor's Adult ADHD Rating Scales

DAT – Dopamine transporter

FSIQ – Full scale intelligence quotient

MPQ – Multidimensional Personality Questionnaire

NAT – Noradrenaline transporter

NART – National Adult Reading Test

SN – Substantia nigra

SNpc – Substantia nigra pars compacta

SNpr – Substantia nigra pars reticulata

TD – Temporal Difference

TPQ - Tridimensional Personality Questionnaire

VTA – Ventral tegmental area

Acknowledgements

Massive love and thanks to all the patients and volunteers who took part in the study. Getting to know all of you was an absolute pleasure. Thank you to the radiographers of CISC, past and present. You kept me going through the dark mornings, button-box failures, and quenches. Thank you Mara. You've taught me so much there aren't enough words on a page to express my gratitude. You've been endlessly compassionate and inspiring, and reassured me that science can be light-hearted, friendly and apolitical. Neil, thank you for always pushing me to explore more, teaching me how to survive in academia, and showing me that sometimes it's just better to buy a new sofa-bed rather than trying to haul one down from London. Thank you Ella and Pat for being the bright smile that I've needed after a long commute. Kate, thank you for keeping me going through all of this. Sharing the excitement, anxieties and panics of research with you has meant so much. Finally, thank you to my Mum and Dad, and the rest of my family that extends far beyond conventional borders. Without your love and support I'm not sure how I would've survived this world. I would be nothing without you.

Recruitment, participant testing, coding of experimental paradigms, data analysis, and writing were performed by me under the supervision Mara Cercignani and Neil Harrison. Additional assistance with recruitment was provided by the staff of the Sussex Partnership NHS Foundation Trust. Edwin Evelyn-Rahr also contributed to VBM analyses in Chapter 3. Mara Cercignani and Neil Harrison were responsible for designing scanning protocols and deciding on experimental paradigms.

Declaration

I declare that the research contained in this thesis, unless otherwise formally indicated within the text, is the original work of the author. The thesis has not been previously submitted to this or any other university for a degree, and does not incorporate any material already submitted for a degree.

Signed:

Dated: 05/06/2016

1 Introduction

Attention Deficit Hyperactivity Disorder (ADHD) is diagnostically categorised according to the presence of inattentive, hyperactive and impulsive symptom domains, and is the most common neurodevelopmental disorder, with an estimated prevalence of approximately 5% (Polanczyk et al. 2007). These symptoms persist into adulthood fully in around 15% of cases, and partially in 65% (Faraone et al. 2006), with a suggested prevalence of around 2.5% of the adult population (Simon et al. 2009). This persistence of symptoms can have highly deleterious consequences to both the individual and society, being associated with reduced employment, difficulty in interpersonal relationships, increased drug use, serious transport accidents and incarceration (Harpin 2005; Rösler et al. 2004; Chang et al. 2014). As acknowledgement of these issues, research into the neurobiology of ADHD in adulthood has been gaining momentum.

ADHD has largely been considered to be a disorder of the brain dopamine system. Whilst this was initially inferred from the efficacy of dopamine enhancing psychostimulants in the disorder, a wealth of genetic (Gizer et al. 2009; Franke et al. 2012) and molecular imaging studies (Volkow et al. 2007; Volkow et al. 2009; Volkow et al. 2012; Fusar-Poli et al. 2012; Volkow et al. 2011; Badgaiyan et al. 2015) now support this hypothesis. In spite of this, the precise nature of anatomical and functional abnormalities within the dopamine system, and how they are targeted by medication, remains unclear. Even some of the most widely reported findings in childhood such as differences in striatal morphology are poorly replicated in adulthood (Frodl & Skokauskas 2012; Nakao et al. 2011). This has led to suggestions that these anatomical abnormalities remit with development, even when symptoms persist. The question of whether these persistent cases reflect a dopaminergic deficit, or have some other neurobiological basis is unclear (del Campo et al. 2013).

Similarly, whilst there has been extensive work examining the morphology of networks modulated by dopaminergic signalling in ADHD, little is known of the role of the substantia nigra/ventral tegmental area (SN/VTA) which is at the heart of dopaminergic modulatory function. Though work has examined how reward networks are functionally altered in ADHD, the mechanisms underlying abnormal reward function, and its rescue by medication, is relatively poorly understood.

With the development of novel imaging methodologies and computational theories of dopaminergic function, identifying precise pathological and therapeutic targets of the brain dopamine system has become increasingly possible. The purpose of this work is to employ these advancements to resolve certain outstanding questions about the neurobiology and treatment of ADHD. This introductory segment will describe the neuroanatomical and functional context of these questions. Following this, three experimental chapters will introduce these problems and approaches in greater detail. In brief, these chapters will address:

i. The inadequacy of current imaging methods for visualising subcortical structures, and how updating these methodologies may shed light on previous conflicting reports about striatal abnormalities in ADHD
ii. How different subcomponents of the SN/VTA contribute to reward phenotypes observed in ADHD, namely reduced incentive motivation and increased waiting impulsivity, and how these subcomponents are altered by long term medication use
iii. How changes in computational mechanisms result in altered reward learning in ADHD, with a focus on stimulus novelty. This chapter will model these computational parameters against behaviour and functional imaging data, and assess how they are affected by acute treatment with stimulant medication

1.1 ADHD: Background

1.1.1 Diagnosis

ADHD is diagnosed according to the presence of clinically significant inattentive and/or hyperactive and impulsive symptom clusters that are observed in two or more settings (American Psychiatric Association 2013). ADHD is presently subcategorised into inattentive, hyperactive/impulsive and combined presentations (or 'subtypes', in DSM IV nomenclature) according to the presence of 6 or more symptoms of each respective domain (Table 1.1) in childhood, and 5 or more in adulthood. In response to a growing need to understand and treat the persistence of these symptoms in adulthood (Ginsberg et al. 2014), various changes from the DSM IV criteria have been adopted. In particular, reduced symptom count requirements in adults reflect the tendency for symptoms, particularly within hyperactive/impulsive domains, to reduce with age

(Biederman et al. 2000). The required presence of symptoms only before the age of 12 (rather than 7) also serves as a marked shift in recognising the prevalence of later onsets of the disorder. Additionally, the necessity for 'clinically significant impairment' in two or more settings has shifted to a requirement that symptoms 'interfere' with function and are 'present' in two more setting. Both DSM IV and V require that symptoms not be present exclusively during the course of schizophrenia or other psychotic disorder, or are not better explained by another disorder. The DSM V criteria removes the requirement that symptoms do not arise during another pervasive developmental disorder, allowing for joint diagnoses of ADHD and Autism Spectrum Disorders (ASD) that would not previously been permitted. Finally, the DSM V encourages more specific sub-threshold diagnoses in cases where full criteria are not met, but clinically significant impairments that warrant diagnoses and treatment are observed. In particular, the introduction of light, moderate and severe symptom ratings are intended to be used to descriptively supplement a diagnosis of 'Other specified ADHD'.

Table 1.1 DSM V criteria for inattentive and hyperactive impulsive presentations

Inattentive presentation	Hyperactive/Impulsive presentation
Fails to give close attention to details or makes careless mistakes	Fidgets with hands or feet or squirms in chair
Has difficulty sustaining attention	Has difficulty remaining seated
Does not appear to listen	Runs about or climbs excessively in children; extreme restlessness in adults
Struggles to follow through on instructions	Difficulty in engaging in activities quietly
Has difficulty with organisation	Acts as if driven by a motor; adults will often feel inside like they were driven by a motor
Avoids or dislikes tasks requiring a lot of thinking	Talks excessively
Loses things	Blurts out answers before questions have been completed
Is easily distracted	Difficulty waiting or taking turns
Is forgetful in daily activities	Interrupts or intrudes upon others

1.1.2 Persistence of ADHD into adulthood

ADHD is thought to affect around 5% of children (Polanczyk et al. 2007) and in both childhood and adulthood appears to disproportionately affect the male population (Willcutt 2012). In spite of popular assertions that the disorder is a westernised social construct, ADHD prevalence is equivalent across cultures (Faraone et al. 2003; Polanczyk et al. 2007), with variance in this likely explained by different diagnostic methodologies (Polanczyk et al. 2007). In particular, failure to apply the requirement of functional impairment in two settings can greatly alter diagnoses, which is highly problematic in studies using self-report diagnostic methods.

The persistence of ADHD into adulthood appears to show far greater variation than childhood (Simon et al. 2009). Follow-up studies, for example, appear to suggest a range of 4-66% cases persisting into adulthood. As in childhood studies this appears to reflect differences in diagnostic methodologies, with the increased reliance on self-report measures in adulthood likely explaining the greater variance in prevalence reported (Simon et al. 2009). This problem is compounded, however, by a tendency to treat ADHD symptoms as secondary to other comorbidities in adulthood (Ginsberg et al. 2014; Fayyad et al. 2007). As ADHD symptoms alter with maturation, they may be more subtle and less readily detected using previous DSM IV criteria (Kooij et al. 2010). For instance, whilst motor hyperactivity may wane in the disorder (Biederman et al. 2000), hyperactive symptoms can manifest in adults as feelings of inner or mental restlessness (Weyandt et al. 2003). Problematically, whilst adult ADHD most commonly takes the form of the predominantly inattentive subtype, those with combined subtype are significantly more likely to be referred to clinical services population (Willcutt 2012). Time will be required to determine whether changes in the DSM V aimed at assisting ADHD diagnosis in adulthood will reduce this variance.

1.1.3 Genetics of ADHD

Family and twin studies of childhood ADHD report a heritability of around 70-80% (Faraone et al. 2005). Heritability studies in adulthoods had initially suggested a lower heritability (~30-40%), although this too likely reflects an increased reliance on self-report measures (Franke et al. 2012). More recent evidence using psychiatric diagnoses (using the ICD-10, rather than DSM) has shown a heritability of around 88%

across the lifespan (Larsson et al. 2014). Most studies examining genetic contributions to ADHD have focussed on dopamine system encoding genes, of which the dopamine receptor DRD4 and DRD5, and dopamine transporter (DAT) encoding genes, are highly implicated (Gizer et al. 2009; Franke et al. 2012; Hawi et al. 2015). So far several studies have investigated the relationship between DRD4 and DAT polymorphisms and brain structural and function. For instance, studies have showed that DRD4 polymorphisms associated with ADHD are linked to thinning of the right orbitofrontal/inferior prefrontal and posterior parietal cortex (Shaw et al. 2007), dorsolateral prefrontal and cerebellar cortex (Monuteaux et al. 2008), and prefrontal cortex (Durston et al. 2005), whilst DAT1 polymorphisms associated with ADHD have been linked to the volume of the caudate nucleus (Durston et al. 2005). Functional imaging tasks have also shown highlighted links between activation of the striatum during response inhibition, DAT1 genotype and familial expression of ADHD (Durston et al. 2008; Bédard et al. 2010). Overall, both DAT1 and DRD4 polymorphisms have been linked to neuroanatomical and functional changes associated with ADHD (with the bulk of studies focussing on these genes (Durston 2010)).

Other genes that share prominent interactions with the dopamine system have also been implicated. For instance, nitric oxide synthase (NOS1) polymorphisms (Hoogman et al. 2011; Hawi et al. 2015) have been detected which may alter the inhibitory role of nitric oxide at the dopamine transporter (Kiss et al. 2004). Similarly, LPHN3 (a latrophilin family G protein coupled receptor gene) polymorporphisms are associated with ADHD (Franke et al. 2012; Hawi et al. 2015), and result in abnormal dopamine neuron development and ADHD like behaviours in animal models (Lange et al. 2012). Synaptosomal associated protein-25 (SNAP-25), serotonin system, and noradrenaline system encoding genes have also been strongly implicated in candidate gene studies (Hawi et al. 2015).

Such individual genetic contributions to ADHD do however appear to be of modest size, and genome wide association studies (GWAS) have had limited success in identifying candidate genes at stringent thresholds (Hawi et al. 2015). The genetic heterogeneity in ADHD has, as in most psychiatric disorders, limited inference as to any shared dysfunctional molecular pathways. More recent network analyses may help resolve these questions and point to how alterations to different genes of small effect can contribute to the same dysfunctional pathway. This involves using network analyses of genes previously associated with psychiatric disorders to model the functional domains in which they commonly interact. The functional molecular

pathways or 'modules' that are impacted in disorders can therefore be directly assessed, rather than focussing on the contribution of a single gene that may contribute to multiple such pathways. This has the benefit of examining how the range of genes of small effect that are associated with a disorder may individually and cumulatively contribute to a similar phenotype, whilst also accepting the heterogeneity of individual polymorphisms associated with psychiatric diagnoses. Such network analyses in ADHD have, for instance, implicated genes contributing to synaptic transmission, catecholamine metabolism, G-protein signalling pathways and cell migration in ADHD (Cristino et al. 2014). However, whilst the study of psychiatric genetics has moved towards these more complex approaches these have yet to be tested in terms of their effect on functional neuroanatomy. Future studies will be required to determine how such pathway models are linked to imaging data as a priori candidate genes have been (Durston 2010).

1.1.4 Stimulant medication in ADHD

Current first line treatment of ADHD consists of either methylphenidate or various formulations of amphetamine. Within the different formulations of amphetamine, in the UK, the dextrorotatory enantiomer D-amphetamine is typically used due to its increased potency in eliciting dopamine release and blocking its reuptake (Patrick & Markowitz 1997), as well as showing greater levels of symptom improvement when compared to L-amphetamine or racemic mixtures (Arnold et al. 1972; Gross 1976). Racemic and other mixed (typically 75% D-amphetamine, 25% L-amphetamine) are also used, however. More recently, the inactive prodrug lisdexamphetamine has also been used, which is converted to D-amphetamine in a manner that is rate limited by enzymatic cleavage of L-lysine over the course of approximately 12 hours (Blick & Keating 2007).

Methylphenidate acts primarily as a dopamine transport (DAT) reuptake inhibitor with some inhibitory actions at noradrenergic reuptake (NAT) sites (Wall et al. 1995). Amphetamine's primary actions appear to be competitive and non-competitive DAT uptake inhibition, and releasing vesicular dopamine into the cytosol whilst also promoting DAT mediated reverse transport of this dopamine into the synaptic cleft (Fleckenstein et al. 2007). Whilst both drugs also have some affinity for other dopaminergic, noradrenergic and serotonergic sites, their primary therapeutic

mechanism of action is considered to be increasing dopamine concentration in the synaptic cleft (Seeman & Madras 1998). Indeed, the dopamine increasing properties of both amphetamine and methylphenidate are orders of magnitude greater than their effects on noradrenaline and serotonin (Kuczenski & Segal 1997; Easton et al. 2007). At the low doses that are typically used to treat ADHD this enhances levels of tonic dopamine but reduces impulse-induced phasic dopamine release relative to tonic levels, ostensibly due to increased D2 receptor mediated inhibition of dopaminergic neurotransmission (Figure 1.1) (Dreyer et al. 2010; Seeman & Madras 1998). Accordingly, increased dopamine binding to D2/D3 receptors induced by methylphenidate has been observed to be predictive of symptom improvement (Volkow et al. 2012).

The half-life of methylphenidate is 2-3 hours, with peak plasma time achieved in around 2 hours. The duration of peak action is around 2-4 hours for instant release, 3-8 for sustained, and 8-12 for extended release methylphenidate (Kimko et al. 1999). The half-life of D-amphetamine is around 9-11 hours, with peak plasma levels occurring at 3 hours (United States Food and Drug Administration 2013).

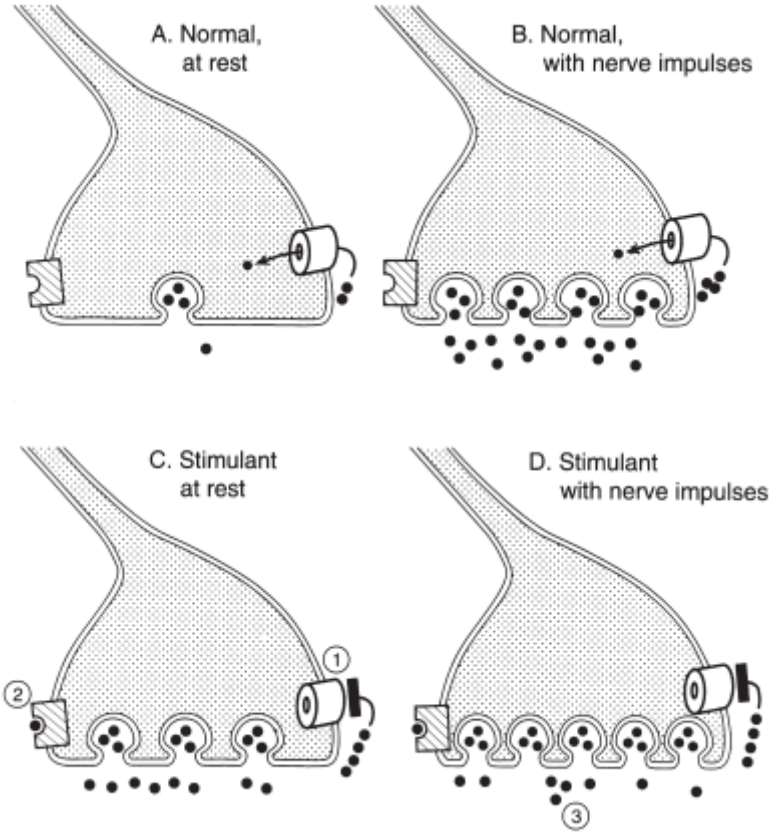

Figure 1.1 Effects of stimulant medication on synaptic dopamine. Reproduced from (Seeman & Madras 1998).

By blocking DAT reuptake of dopamine (1), Stimulant medication increases synaptic tonic dopamine levels (C) relative to normal (A) conditions. Presynaptic inhibitory D2 receptors (2) are preferentially activated by this stimulant-induced increase in tonic dopamine levels, reducing phasic (3) dopamine release in response to stimulation (D) when compared to unmedicated conditions (B).

1.2 Neurobiology of ADHD

1.2.1 ADHD as a disorder of the dopamine system

Brain dopamine plays a central regulatory role in a range of functions that extend from the goal-directed motor functions for which it was initially ascribed, to the emotional, motivational and cognitive processes that drive them. Despite this large functional repertoire, dopaminergic cells make up only around 590,000 neurons in the brain (Chinta & Andersen 2005), approximately 90% of which are located within the dopaminergic midbrain, or SN/VTA. These neurons control motor, cognitive and motivational functions through extensive projections that terminate within the striatum, but also other subcortical regions such as the amygdala and hippocampus, and the cortex. These midbrain projection systems have typically been subdivided into mesolimbic projections terminating in the ventral striatum (as well as amygdala and hippocampus), nigrostriatal projections terminating in the dorsal striatum, and a mesocortical projection system that sends diffuse projections the cerebral cortex. Finally, a tubero-infundibular system projects from the tuberal hypothalamus to the pituitary gland (Figure 1.2).

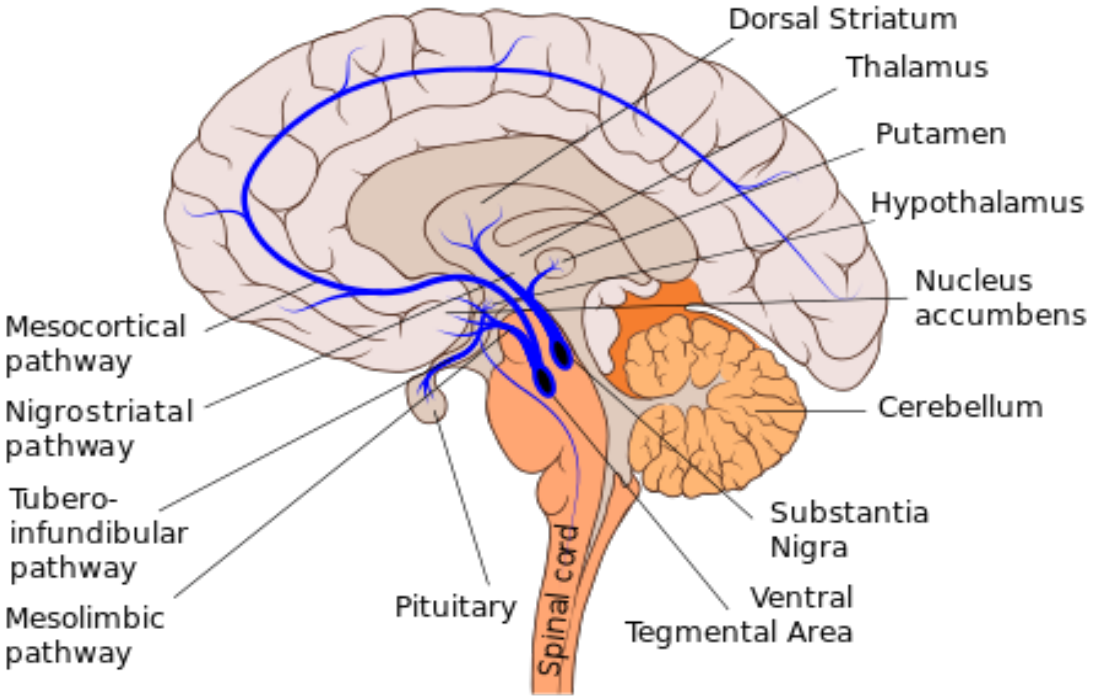

Figure 1.2 Dopamine projection systems depicting mesolimbic, mesocortical, nigrostriatal and tubero-infundibular pathways.

Various lines of evidence have suggested the importance of dopaminergic dysfunction in ADHD. In particular, molecular imaging studies have consistently highlighted the importance of reduced D2/D3 receptor and dopamine transporter (DAT) binding potentials in the disorder (Volkow et al. 2009). Such studies have shown convergence with genetic evidence, where polymorphisms in DAT1, DRD4, and DRD5 have been fairly consistently detected in ADHD samples (Gizer et al. 2009). The most commonly identified locus of these molecular abnormalities has been within the striatum (Volkow et al. 2007; Volkow et al. 2009; Volkow et al. 2011; Volkow et al. 2012; Badgaiyan et al. 2015), and additionally the SN/VTA (Volkow et al. 2011; del Campo et al. 2013) and its connected limbic regions (Volkow et al. 2007). Importantly, such abnormalities in dopaminergic neurotransmission appear to be associated with both inattentive (Volkow et al. 2007; Volkow et al. 2009) and hyperactive/impulsive symptoms (Rosa Neto et al. 2002).

1.2.1.1 The nature of dopamine deficits in ADHD

The precise nature of dopaminergic abnormalities within ADHD have however been widely debated. Most broadly, ADHD has been considered to be a disorder characterised by low levels of brain dopamine (Volkow et al. 2005). However, others have suggested a more nuanced account.

For instance, the dynamic development theory DDT posits that low levels of tonic dopamine specifically explain key observations within ADHD, such as a steeper delay-of-reinforcement gradients (i.e. increased temporal discounting, described below), and slower extinction effects in reinforcement (Sagvolden et al. 2005). The dopamine transfer deficit (DTD) theory alternatively focusses on altered anticipatory firing to predictors of reward (Tripp & Wickens 2008). During normal learning, phasic dopamine firing is understood to shift from an unexpected reward to the cue signalling that reward. In ADHD, it is suggested that this transfer of phasic reward signalling fails to fully occur. As such the predictor of reward is signalled only partially, whilst the actual reward itself continues to elicit dopamine cell firing which would subside in normal learning. This theory also predicts critical neuropsychological components of ADHD such as increased temporal discounting. Other neurochemical models of dopamine dysfunction in ADHD have focused on the relative contributions of phasic and tonic dopamine (Cherkasova et al. 2014; Badgaiyan et al. 2015). Specifically, it has been suggested that that whilst tonic dopamine is reduced in the disorder, phasic dopamine is actually increased. This may also make sense of prior divergent findings that have

suggested both increased and decreased D2/D3 receptor binding potentials in ADHD (Cherkasova et al. 2014; Badgaiyan et al. 2015). It should be noted that these theories are not necessarily mutually exclusive. For instance, DTD and high-phasic/low-tonic theories could well dovetail. Future molecular work is required to resolve these neurochemical theories of dopamine abnormalities in ADHD (though see the discussion in Chapter 5 for further, albeit speculative, evidence). Other critical findings supporting the importance of dopamine systems in ADHD reflect functional and anatomical s within the core and extended structures within the dopaminergic system which are reviewed in the following sections.

1.2.1.2 The critical role of core and extended dopaminergic cortico-striato-thalamo-cortical networks to ADHD pathophysiology

In line with the weight of evidence linking dopaminergic molecular abnormalities to the striatum, morphometry studies have robustly linked childhood ADHD to striatal volumetric reductions and an extended cortico-striato-thalamo-cortical network (Castellanos et al. 2006; Almeida Montes et al. 2010; Seidman et al. 2011; Frodl & Skokauskas 2012; Nakao et al. 2011; Seidman et al. 2005; Valera et al. 2007; Batty et al. 2015; Ivanov et al. 2010; Proal et al. 2011; Xia et al. 2012; Stanley et al. 2008). These remarkably organised circuits process and regulate an axis of motivational – cognitive – motor functions through a set of parallel, looping circuits that also integrate and feed forward information between these functions. This functional axis is anatomically distributed over a ventromedial to dorsolateral gradient within each of the structures this loop comprises (Haber 2003) (Figure 1.3).

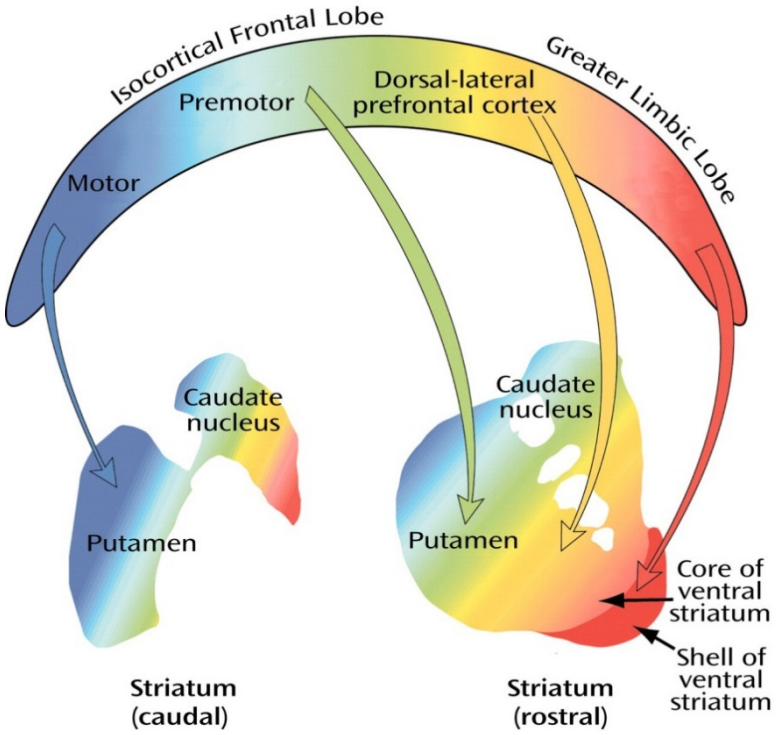

Figure 1.3 Gradients of cortisco-striatal connectivity. Reproduced from (Heimer 2003).

A gradient of ventromedial (red) – dorsolateral (blue) connectivity within the cortex and striatum represents parallel limbic, associative and motor networks. The red – blue gradient provides an illustration of how distinct functions are localised with the same structure. The red here represents the ventromedial components underpinning motivational functions, with yellow and green representation more dorsolateral regions with cognitive and associative functions. The blue segments represent the most dorsolateral subregions within these structures and are responsible for motor function. Overlapping projections within these regions allow integration of these processes. Reproduced from (Heimer 2003). This figuratively represents

Due to the breadth of functions associated with these loops, abnormalities within them have vast explanatory power for the numerous deficits associated with ADHD (Castellanos et al. 2006). For example, differences in orbitofrontal and ventral striatal regions are linked to reward dysfunction in ADHD (Scheres et al. 2007; Wilbertz et al. 2012; Rubia et al. 2009; Cubillo et al. 2012; Carmona et al. 2009; Hesslinger et al. 2002). Similarly, abnormalities in lateral frontal regions, as well as the dorsolateral striatum, have been linked to more traditionally 'cognitive' deficits in the disorder, such as attention and executive functioning (Cubillo et al. 2012; Depue, Burgess, Bidwell, et al. 2010; Depue, Burgess, Willcutt, Ruzic, et al. 2010; Depue, Burgess, Willcutt, Bidwell, et al. 2010).

Within the context of this cortico-striato-thalamo-cortical model, striatal abnormalities provide a key locus of dopaminergic dysfunction within this network which may play a primary role in the disorder, emerging prior to other neurobiological abnormalities (Stanley et al. 2008). In addition to the wealth of genetic studies linking ADHD to dopamine system encoding genes (Gizer et al. 2009; Franke et al. 2012), the prominence of childhood striatal abnormalities in a disorder that is otherwise marked by a large amount of neurobiological heterogeneity suggests this may well be the case. Interestingly, volumetric reductions within the striatum may represent a locus of neurobiological divergence between childhood ADHD and adulthood, where such abnormalities are less frequently detected (Nakao et al. 2011; Frodl & Skokauskas 2012). Chapter 3 addresses these issues in more detail, examining whether this reflects maturation and treatment related normalisation (Nakao et al. 2011) or if other, methodological factors, may account for this. Supporting this, the following section reviews morphological findings in ADHD, highlighting commonalities and areas of divergence between childhood and adult populations.

1.2.1.3 Morphological findings in childhood and adulthood ADHD implicate core dopaminergic/striatal and extended cortico-striato-thalamo-cortical abnormalities

Voxel-based morphometry (VBM) studies have offered a method of exploring structural brain abnormalities in a manner unconstrained by prior hypotheses. Meta-analyses of

VBM studies in childhood ADHD have confirmed the importance of striatal regions, in particular including reductions in the right putamen (extending to the globus pallidus) (Ellison-Wright et al. 2008; Frodl & Skokauskas 2012). ROI based meta-analyses have also implicated the caudate in childhood ADHD (Valera et al. 2007; Frodl & Skokauskas 2012). Though striatal abnormalities are rarely detected in whole brain adult ADHD analyses, ROI based studies have observed striatal abnormalities in ADHD (Seidman et al. 2011; Almeida Montes et al. 2010). Interestingly, one study that did detect whole-brain statistically corrected abnormalities in adult ADHD had followed up these patients from a childhood diagnosis (Proal et al. 2011). A recent study focusing on stimulus naïve adults suggested that caudate volumetric reductions are observed in adult ADHD, though these did not survive correction for multiple comparisons (Nikos Makris et al. 2015). The reduced prominence of striatal abnormalities in adult samples is consonant with independent studies and meta-analyses have suggested that both maturation and medication may normalize striatal volumes in ADHD (Nakao et al. 2011).

Other morphological abnormalities have also been observed in childhood, albeit not with the levels of replication to be implicated in meta-analytic studies. For instance, reduced hippocampus volume and amygdala surface area has been observed (Plessen et al. 2006), as well as thalamic morphological abnormalities (Ivanov et al. 2010). Specifically, reduced pulvinar volumes are observed in ADHD compared to controls and general thalamic and pulvinar volumes specifically appear to be increased by stimulant medication. Volumetric reductions of the lateral thalamic surface appears to be associated with hyperactivity symptoms, whilst increased volume of the medial thalamic surfaces appeared to associated with inattentive symptoms (Ivanov et al. 2010). The persistence of thalamic abnormalities into adulthood has been supported by longitudinal studies (Proal et al. 2011). Evidence for hippocampal volumes in adulthood has however been limited (Perlov et al. 2008) though some studies have detected changes at lenient statistical thresholds (Seidman et al. 2011). Similarly, findings implicating amygdala abnormalities in adulthood have been mixed (Perlov et al. 2008; Frodl et al. 2010), though given the limited amount of evidence implicating these regions in childhood, it is not possible to infer the likelihood of maturational effects.

Abnormal cerebellar volumes have also been consistently reported in childhood (Valera et al. 2007) and adult ADHD (Nikos Makris et al. 2015). Whilst the nature of cerebellar abnormalities has largely been ignored, a recent study implicated the cerebellar

subregions found to be abnormal in ADHD (lobule IX) to be regions interacting with ventral and dorsal attention networks (Stoodley 2014).

Within the cortex, abnormal volumes in prefrontal and premotor regions (Mostofsky et al. 2002), the supplementary motor area (SMA) and primary somatosensory areas (Duerden et al. 2012),the temporal lobe (Kobel et al. 2010), the anterior insula (Lopez-Larson et al. 2012), and the anterior cingulate cortex (ACC) (Semrud-Clikeman et al. 2006) have been found in children. Cortical thickness studies have also shown thinning effectively across the whole cortex, though this appears to be most pronounced in medial prefrontal regions (Shaw et al. 2006; Narr et al. 2009). In adulthood, individual studies generally reflect cortical findings in childhood, with abnormalities observed in right inferior frontal (Depue, Burgess, Bidwell, et al. 2010), dorsolateral prefrontal cortex, ACC (Seidman et al. 2006; Makris et al. 2007), inferior parietal lobe (Makris et al. 2007), orbitofrontal cortex (Hesslinger et al. 2002). Interestingly, ACC reductions observed in children have been suggested to be normalised by stimulant medication (Semrud-Clikeman et al. 2006). This appears to be at odds with findings from a meta-analysis of adult patients with ADHD, most of whom had been treated with stimulant medication, which found consistent volumetric reductions in the ACC (Frodl & Skokauskas 2012).

In summary, frontal and cerebellar reductions appear to be consistent across both childhood and adulthood, though other cortical, amygdala, hippocampal and thalamic alterations may differ. However, given the heterogeneity in findings even between studies in the same age group it is hard to draw conclusions about any developmental or treatment related effects. In contrast, striatal abnormalities are consistently detected in childhood but not in adulthood. Some evidence suggests that this may reflect medication and maturation effects, and Chapter 3 will assess these claims more closely.

1.2.1.4 Evidence for SN/VTA involvement in ADHD

Abnormal dopaminergic signalling is central to most neurobiological theories of ADHD (Luman et al. 2010). Whilst the SN/VTA is the core of the dopaminergic system, its direct role in ADHD pathophysiology is relatively unknown largely due to limitations in non-invasive imaging of the dopaminergic midbrain. Recent work has now directly

implicated the SN/VTA in ADHD. Still, there has been a paucity of studies examining the precise functional contribution of the SN/VTA and its subcomponents. For instance, increased echogenicity of the substantia nigra has been observed in children with ADHD using transcranial sonography (Romanos et al. 2010). However, inference as to the neurobiological differences underpinning these changes is limited. More recently, molecular imaging studies (Volkow et al. 2011; Buckholtz et al. 2010) have suggested that D2/D3 receptor binding densities in the SN/VTA may underpin essential components of ADHD.

Abnormal incentive motivation is increasingly recognised as a potentially central aetiological component in ADHD (Volkow et al. 2011; Silvetti et al. 2013). Recent findings indicate that dysfunctional SN/VTA reward pathways result in a motivational deficit in ADHD, and these may underpin inattentive symptoms in the disorder (Volkow et al. 2011). Similarly, D2/D3 receptor activity in the SN/VTA appears to encode a tendency towards impulsivity in the general population (Buckholtz et al. 2010). Whilst impulsivity is a multifaceted construct (Caswell et al. 2015), research in ADHD has specifically highlighted the relevance of waiting impulsivity, most typically in the form of increased temporal discounting (Thorell 2007; Scheres et al. 2008; Scheres et al. 2010). This tendency to prefer smaller, immediate rewards over larger temporally distant ones, appears to be a fundamental part of reward dysfunction in ADHD (Luman et al. 2005; Sonuga-Barke et al. 2008). Whilst preliminary evidence suggests that the SN/VTA has a role in both impulsivity and motivation, it is not clear how the subcomponents of the SN/VTA contribute to these different aspects of reward dysfunction.

1.2.1.5 Substantia nigra/ventral tegmental area heterogeneity

The SN/VTA is a highly heterogenous structure that is subdivisible at several different levels. Similar to the striatal structures which it regulates, a dorsomedial – ventrolateral functional gradient is observed in the SN/VTA. The dorsomedial component comprises the VTA, retrorubal cell groups and a dorsal element of the SN pars compacta (SNpc), and regulates emotional and motivational functions most prominently via mesolimbic projections to the ventral striatum, amygdala and hippocampus (Haber et al. 2000; Haber 2003; Haber & Knutson 2010). Conversely, the ventrolateral SN/VTA regulates a broad range of cognitive, associative motor functions via nigrostriatal projections to the

dorsal and lateral aspects of the striatum. Interestingly, these two components also show a range of differences in their pharmacological responses, with different reactivity to D- and L-amphetamine (Browder et al. 1981) and selective D3 (Ashby et al. 2000) and D1 receptor ligands (Goldstein & Litwin 1988), as well as serotonergic (Gervais & Rouillard 2000), noradrenergic (Mejías-Aponte et al. 2009) and nicotinic acetylcholinergic (Mereu et al. 1987; Klink et al. 2001) signalling.

Previous studies investigating the role of the SN/VTA in ADHD have not had sufficient anatomical resolution to dissociate the contributions of these mesolimbic and nigrostriatal components. The midbrain and striatal correlates of incentive motivation in particular remain unclear. Whilst initial accounts have suggested that the mesolimbic SN/VTA and the ventral striatum underpinned incentive motivation, recent evidence has suggested that motivational differences are related to the nigrostriatal SN/VTA (Rossi et al. 2013) and more dorsal aspects of the striatum (Volkow et al. 2002; Tomer et al. 2008). Chapter 4 optimises and applies subcortical imaging and parcellation techniques to address these questions.

1.2.2 Other network dysfunctions in ADHD

With the advent of functional connectivity analyses of resting state fMRI data, there has been an increasing focus on characterizing effects of ADHD on functionally-derived large scale brain networks. In particular, default-mode, fronto-parietal and dorsal and ventral attention networks have been suggested to play a key role in ADHD neurobiology (Castellanos & Proal 2012).

1.2.2.1 Fronto-parietal network

Abnormalities within a fronto-parietal 'control' network, which includes the lateral frontal, anterior cingulate (ACC), dorsolateral prefrontal cortex (DLPFC), anterior PFC (apFC), lateral cerebellum, anterior insula, caudate, and inferior parietal lobe (Figure 1.4) (Vincent et al. 2008), have been suggested to play an important role in ADHD (Castellanos & Proal 2012). Consonant with executive dysfunction in the disorder, this network appears to play a role in orchestrating goal-directed behaviours and adapting

to shifting environmental demands (Liston et al. 2006). In addition to regional hypoactivations during go/no go, response inhibition, attention, working memory and time discrimination tasks (Bush 2010; Vaidya & Stollstorff 2008; Schneider et al. 2006; Smith et al. 2008; Durston et al. 2007; Rubia 2011), abnormal functional connectivity within this network has also been detected in resting state studies (Cao et al. 2006; Yu-Feng et al. 2007; Wang et al. 2009; Cao et al. 2009).

1.2.2.2 Dorsal and ventral attention networks

The dorsal and ventral attention networks work in concert to regulate attention. The ventral attention network is involved in monitoring the environment for salient stimuli and may, in response to this, have a role in interrupting top-down attentional processing to induce an re-orienting response (Corbetta et al. 2008). This ventral attention network overlaps with functionally derived salience/fronto-opercular networks (Menon 2011; Dosenbach et al. 2008), and encompasses the temporoparietal junction, frontal operculum, anterior insula, and ventral frontal regions including the middle and inferior frontal gyri (Corbetta et al. 2008). By contrast, the dorsal attention network mediates top-down reorientation of attention and other goal-direction functions in response to competing demands. This network consists largely of superior parietal regions, including the intraparietal sulcus and superior parietal lobule, and dorsal frontal regions focused on the frontal eye field (Figure 1.4) (Corbetta et al. 2008). Abnormal activation patterns in insula, parietal and frontal regions associated with attention networks has been observed in ADHD during a variety of tasks (Dickstein et al. 2006). In addition to the apparent top-down control deficits in ADHD implicating the dorsal attention network specifically (Castellanos & Proal 2012), recent theoretical work has also proposed a specific role of ventral attention network hyperactivity in producing distractability in ADHD (Aboitiz et al. 2014).

1.2.2.3 Default-mode network

The default-mode network (DMN), and its interaction with other networks has been consistently implicated in ADHD. The default-mode network consists of medial prefontal cortex (mPFC), posterior cingulate cortex (PCC) (Figure 1.4), and the medial temporal lobe (MTL). Due to its association with reflection and self-referential processes, the DMN is highly active at rest, and reduced when engaging in most goal-

directed tasks (Buckner et al. 2008). As such, the DMN has an opposing, anticorrelated role in relation to control networks implicated in ADHD. Increased DMN activity during tasks has therefore been argued to reflect a disruption of goal directed processing that could account for momentary lapses in task performance (Sonuga-Barke & Castellanos 2007).

1.2.3 Does functionally derived network dysfunction reflect a primary deficit?

Whilst wide scale disruption to a variety of brain networks in ADHD is observed, it is unclear whether these represent a primary dysfunction, or if they are secondary to reduced dopaminergic function in ADHD. For instance, heightened DMN activity during response inhibition is only observed in patients when they are unmedicated and low motivational incentives are used. By enhancing dopaminergic signalling with either methylphenidate or increased motivational incentive with rewards, heightened DMN activity during tasks is ameliorated (Liddle et al. 2011). These findings suggest that DMN hyperactivity during tasks may actually reflect dysregulation of the DMN and control networks by hypodopaminergic signalling, rather than a discrete primary deficit. Similarly, hypothesised ventral attention network dysfunction is thought to reflect low tonic catecholaminergic signalling (Aboitiz et al. 2014). Overall it is noteworthy, that the functionally derived networks most consistently implicated in ADHD are prominently modulated by dopaminergic nuclei (Cole et al. 2013). As will be discussed below, when examining the effect of dopaminergic reward system contributions to neuropsychological dysfunction, a similar theme emerges.

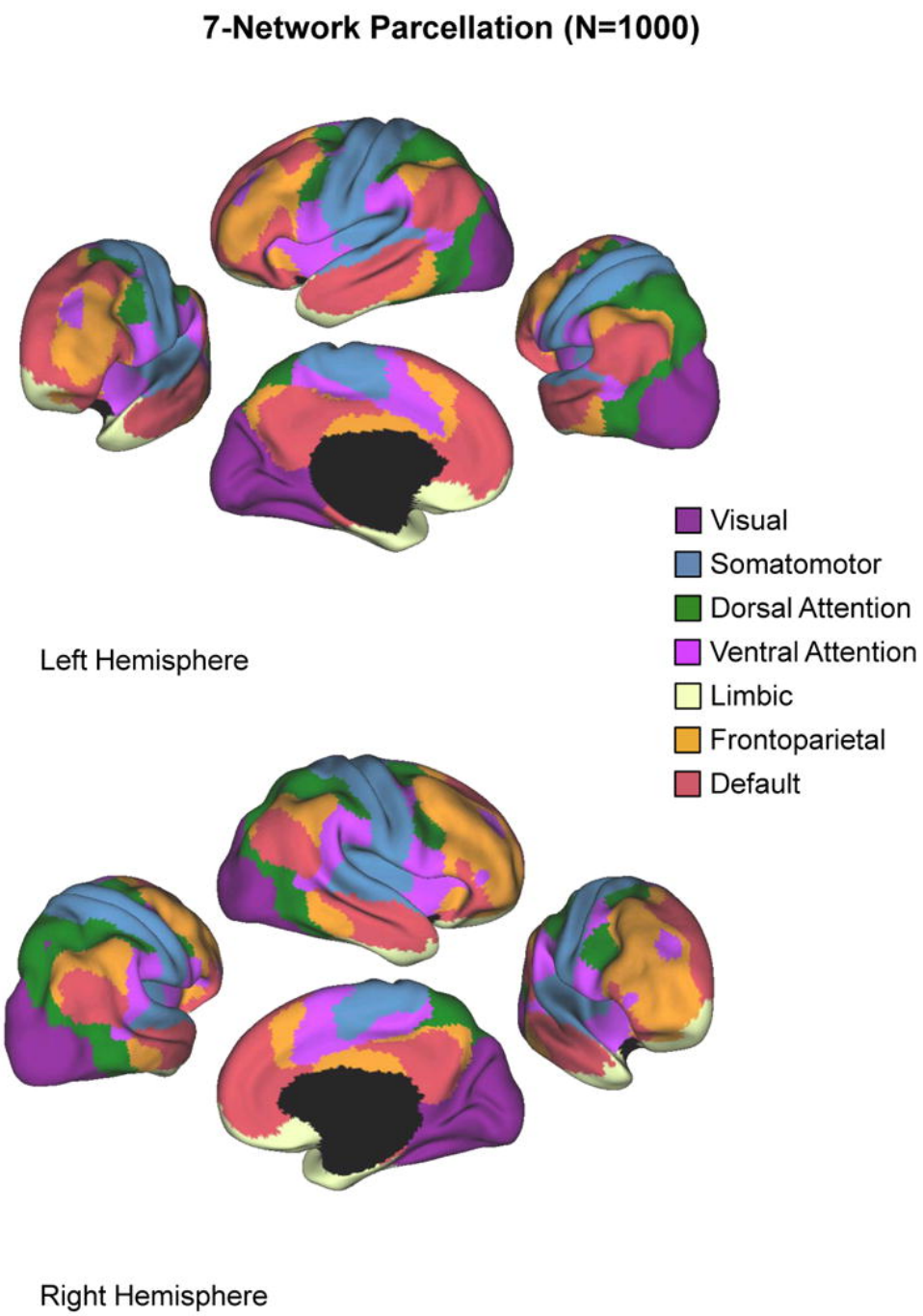

Figure 1.4 Coarse (7-network) parcellation of the human cerebral cortex obtained through clustering of R-fMRI data of 1,000 subjects. Reproduced from (Castellanos & Proal 2012). Initially adapted from (Yeo et al. 2011).

Attention is not a unitary mechanism, but is rather a system supported by several distinct neurocognitive mechanisms. These can be conceptualised as four processes: alerting, orienting, executive control, and self-regulation (Petersen & Posner 2012).

The alerting system appears to be in large part underpinned by noradrenergic signalling from the locus coruleus and is responsible for production and maintenance of optimal vigilance during tasks. The orienting response reflects the direction of attention to a stimulus (Petersen & Posner 2012). This has been shown to reflect two distinct networks, the bottom-up ventral attention network and the top-down dorsal attention network (Corbetta et al. 2008) that have been detailed in previous sections. The executive control contributing toward maintains focus s attention has recently been suggested to reflect two distinct systems (Dosenbach et al. 2008). The first, cingulo-opercular control system acts as a stable background maintenance for task performance, whilst the frontoparietal system (detailed anatomically above) plays a role in initiation and switching of tasks (Dosenbach et al. 2008; Petersen & Posner 2012). Finally, more recent evidence has suggested the importance of a self-regulation system. This reflects the ability to control reflexive or dominant responses to less dominant ones, most typically assessed through use of the Stroop task (Petersen & Posner 2012). In reconciling clinical definitions of attention with neuropsychological criteria, the majority of early research conceptualised attentional deficits as reflecting abnormalities in executive function (subsuming, but not historically limited to the aforementioned networks contributing to executive control of attention).

1.3.2 Executive function in ADHD

As noted, impaired executive function has played a central role in previous definitions of neuropsychological dysfunction in ADHD (Willcutt et al. 2005). Whilst precise characterisation of a 'central executive' in the brain will likely always be problematic, executive function is largely taken to reflect a range of higher order processes that play a role in cognitive, behavioural and emotional regulation. Response inhibition, spatial working memory, vigilance and planning are frequently seen as the best validated measures of executive dysfunction in ADHD (Willcutt et al. 2005), with response inhibition and working memory deficits in particular have been the subject of a large amount of research.

1.3.2.1 Working memory

Working memory, the process by which information no longer in the immediate environment is kept 'on-line' for further processing (Baddeley 2003), has been a considerable focus in ADHD research. Working memory deficits appear to persist into adulthood and have been argued to represent a core deficit in ADHD (Alderson et al. 2013). Methylphenidate treatment improves working memory in both children (Barnett et al. 2001; Mehta et al. 2004) and adults (Ni et al. 2013) with ADHD. These working memory deficits appear to be underpinned by cortico-striato-thalamo-cortical (Mills et al. 2012) and fronto-parietal networks (Darki & Klingberg 2015). Accordingly, enhanced working memory by methylphenidate appears to be underpinned by cerebral blood flow changes within the prefrontal and parietal cortices (Mehta et al. 2000) and enhanced striatal dopaminergic signalling (Clatworthy et al. 2009). These effects of methylphenidate do not, however, appear to be specific to ADHD and have a similarly working memory enhancing effect in healthy controls (Mehta et al. 2000).

1.3.2.2 Response inhibition

The inability to suppress an inappropriate response has been argued to be another central component of executive dysfunction in ADHD (Wodka et al. 2007), and representative of abnormal impulsivity in the disorder. Response inhibition deficits indexed by the stop signal task are ameliorated by methylphenidate (Aron et al. 2003; DeVito et al. 2009) and atomoxetine (Chamberlain et al. 2007), suggesting that acute alteration of dopaminergic and noradrenergic signalling play a therapeutic role. Aberrant response inhibition in ADHD also appears to be underpinned by fronto-striatal abnormalities (Casey et al. 1997; Schulz et al. 2004; Cubillo et al. 2010).

1.3.3 Hot and cool executive dysfunction?

Although executive dysfunction has been linked to the real-life difficulties associated with ADHD (for instance, it appears executive dysfunction has been linked to academic outcomes in ADHD) (Biederman et al. 2004), such executive deficits are frequently absent in the disorder, and do not appear to be necessary or sufficient for its presence (Willcutt et al. 2005). Another prominent line of research in ADHD has focussed on aberrant reward-based decision-making. This has predominantly focussed on well-validated increases in temporal discounting of reward in ADHD (Scheres et al. 2006;

Scheres et al. 2008). This tendency to prefer smaller, more immediate rewards over larger, but temporally distant rewards appears to make distinct contributions from typical executive dysfunction in ADHD (Sonuga-Barke et al. 2003). In addition to other reward-based abnormalities such as risky decision making (Kerr & Zelazo 2004), this has been conceptualised as a form of 'hot' executive dysfunction contrasting to cognitive, or 'cool' executive deficits (Castellanos et al. 2006). This model attempts to encompass the heterogeneity of neuropsychological dysfunction in ADHD, and suggests that both forms of 'executive' dysfunction may reflect abnormalities within cortico-striato-thalamo-cortical loops that appear to play a significant role in the neurobiology of ADHD.

1.3.4 Reinforcement learning

A somewhat opposing view notes that whilst various higher order functions appear to be impacted in ADHD, a great deal of recent work has suggested that these may be underpinned by abnormalities in reinforcement learning (Luman et al. 2010). For instance, previous theories (Castellanos et al. 2006) have suggested that abnormal risk taking and temporal discounting in ADHD represent differences in higher order decision-making functions. However, the level of dysfunction of these processes is not necessarily higher order, and may rather reflect the acquisition and expression of learnt reward values. Contemporary approaches to modelling these reward and decision-making problems have focussed on isolating these factors to assess their individual contributions. For instance, rather than reflecting dysfunction in a unitary, higher-order process, the tendency to prefer smaller more immediate rewards can be described in terms of specific, tightly defined reward learning mechanisms (Williams & Dayan 2005). One prominent approach to these problems has been the application of temporal difference models of reinforcement learning (Sutton & Barto 1998) to behavioural and functional imaging data.

1.3.5 Temporal difference models of reward function

Temporal difference (TD) learning models are a computational approach to reinforcement learning, deriving in part from Monte-Carlo and dynamic programming

methods (Sutton & Barto 1998). Although this approach initially developed within AI research, this has been highly informative about the nature of reinforcement learning in humans and animals, and how accurate reward prediction is possible in the uncertain and changing environments which we inhabit. Moreover, as discussed further below, this has become a fertile ground for exploring reinforcement learning differences that are thought to be abnormal in ADHD. TD models are an approach to learning how to predict future rewards in a constantly updating environment. Specifically, this entails making predictions of a total expected reward value over any number of time steps. In other words, this prediction is intended to capture the total value of picking any given option over a (potentially indefinite) amount of time. At any given time step (for instance, a trial of an experimental task with a win/loss condition on each trial) this uses the error between the reward received and the prior prediction to update the expected reward value. This iterative error-driven learning process (detailed more formally in the equations and their explanations below) thus informs the dynamically perceived values and subsequent decisions of an agent within an environment, offering a computational description of reward related behaviours.

Indeed, such TD models of reinforcement learning have provided a powerful method for characterizing human reward-related behaviour, and have helped clarify mechanisms of reward dysfunction in other disorders of the brain dopamine system (Rutledge et al. 2009; Murray et al. 2008). These TD models are remarkably predictive about the behaviour of dopaminergic neurons in the substantia nigra/ventral tegmental area (SN/VTA) (Bayer & Glimcher 2005; Montague et al. 1996; O'Doherty et al. 2003; McClure et al. 2003; Waelti et al. 2001). Prediction error signals (described below) derived from such models appear to be an essential, quantifiable, measure of reinforcement learning in the brain – both tightly coupled to dopaminergic neuronal activity (Schultz et al. 1997; Hollerman & Schultz 1998), and necessary for learning from reward *in vivo* (Steinberg et al. 2013). In these models, it is possible to decompose discrete computational parameters that affect learning and decision making to assess their individual contributions to these processes. The following sections outline potential parameters of interest and how they may contribute to reward dysfunction in ADHD, with Chapter 5 later empirically addressing these questions.

1.3.5.1 Parameter contributions and derivation of prediction error

In TD models learning is formulated as a process that occurs to predict future reward (Sutton & Barto 1998). At the core of this learning process is the reward prediction error which, in its simplest form, signals the mismatch between an expected reward value *V* at a given time *t*, and the reward received *r*.

$$\delta(t) = r(t) - V(t)$$

In most basic reinforcement learning examples, this value may correspond to the reward value of selecting an option, for instance, the expected value of pulling a lever which is rigged to deliver a reward. In this case, the prediction error signals the difference between the expected value of a lever pull, and the reward received. In turn the prediction error shapes future expectations of reward value as follows:

$$V(t+1) = V(t) + \alpha \bullet \delta(t)$$

This iterative process continually updates the expectations of the agent in response to the state of the environment. Rewards greater than expected will result in a positive predictions error, and increase the predicted value of future rewards. Accordingly, rewards lower than predicted will elicit a negative prediction error, reducing the predicted value of future reward. In this model, the effect of the prediction error on *V* is modulated by the learning rate α, such that a relatively small α will result in slower updating of reward values in response to reward, and bias value predictions to previous experiences. In contrast, a high α will mean that predicted values will be largely informed by the most recent rewards received. Optimal learning strategies therefore balance the weighting given to previous and recent rewards according to the learning rate.

By forming predictions about the values of options in the environment, future decisions can be made on the basis of these value expectations. The assumption underpinning TD models of reinforcement learning, is that a decision making agent is driven to maximize future reward. However, simply consistently selecting options that are perceived to be of the highest value is not an optimal strategy to this end, and is also not descriptive of normal human reward behaviour. This highlights an essential aspect of reinforcement learning, namely that learning and decision making require flexibility, in large part due to the fact that they occur in a dynamic environment. Directing choice solely towards the option with the highest expected value limits exploration of other sources of reward. In an extreme example, given two options of with unknown reward probabilities, an agent that only selected the highest value option would persist

indefinitely in picking the first option that resulted in reward. To overcome this, more sophisticated selection strategies are required, that allow exploration of options that are not perceived to be the most rewarding. One such strategy, softmax selection, gives the probability of choosing a particular option *c* out of a set *k* at time *t*:

$$P(c,t) = \frac{exp(\beta \bullet Q(c,t))}{\sum_{k=1}^{3} exp(\beta \bullet Q(k,t))}$$

In this case, the value is moderated by an inverse-temperature parameter $\boldsymbol{\beta}$ that determines the extent to which choice is directed towards high value options. Differences in $\boldsymbol{\beta}$ thus introduce an element of 'randomness' when deciding whether to pick an option that is perceived to be high value, thus ensuring exploration of other potential sources of reward. In this sense, exploration is required to reduce uncertainty in value predictions.

1.3.6 Modelling mechanisms of reward dysfunction in ADHD

1.3.6.1 Learning rates in ADHD

Preliminary computational modeling work using simulated TD learning in ADHD has indicated several candidate mechanisms to explain impulsive reward dysfunction. Of particular interest, in simulated models altered learning rates have been implicated in ADHD (Williams & Dayan 2005), which have suggested that a reduced rate of updating values in response to reward may explain reward dysfunction observed in the disorder. Reduced learning rates are taken to reflect low dopamine levels in such models (Williams & Dayan 2005). Reduced learning rates in ADHD could therefore potentially tie neurobiological observations of hypodopaminergic abnormalities in mesolimbic reward pathways (Volkow et al. 2009; Volkow et al. 2011) with reward dysfunction that is observed in ADHD (Frank et al. 2007; Thoma et al. 2015; Scheres et al. 2007; Scheres et al. 2006). However, to date no direct evidence of altered learning rates in TD models of ADHD has been observed. Interestingly, impaired learning rates in other hypodopaminergic disorders such as Parkinson's disease are rescued by dopamine-enhancing drugs (Rutledge et al. 2009). Improved learning rates may therefore play a similar role in mediating the effects of stimulant medication in normalizing reward learning abnormalities in ADHD (Williams & Dayan 2005).

1.3.6.2 Exploratation/Inverse temperature parameters in ADHD

Rather than altered acquisition of reward values, another alternative explanation for reward dysfunction in ADHD is altered behaviour towards rewarding options. One recent study provided evidence for heightened inverse temperature parameters (β) in ADHD, reflecting a reduced tendency to exploit options known to be rewarding, instead exploring other options more frequently. Interestingly, this analysis also suggested that learning in ADHD was best characterized by a model assuming fixed learning rates that do not dynamically alter in response to environmental volatility and beliefs about values of objects (Hauser et al. 2014). Comparison with predictions from previous simulations is somewhat difficult however, due to a) the use of a reversal learning paradigm in which the value of options shifted over time, and b) the implementation of non TD models, specifically Rescorla-Wagner (Gläscher et al. 2009) and hierarchical Gaussian filter models (HGF) (Mathys et al. 2011; Iglesias et al. 2013). Rescorla-Wagner models are similar to TD models which have developed from them, but differ on several points. Most importantly, the reward values learnt in Rescorla-Wagner models are applied only to the next timestep (rather than as a predicted value of all future reward from a source). HGF models attempt to apply principles of probability theory into learning problems to overcome the poor performance of TD models where there are environmental states and action outcomes that are unknown to the agent (Mathys et al. 2011).

1.3.6.3 Novelty processing in ADHD

Valuation of novel stimuli may also play a role in abnormal reward function in ADHD, though to date this has been critically underexplored. Novelty has a highly adaptive role in learning and decision making, guiding an agent to explore unfamiliar options to identify new sources of potential reward (Wittmann et al. 2008). In doing this, stimulus novelty itself also elicits phasic dopaminergic activity in the mesolimbic reward system (Schultz 1998). This novelty-related activity can be modelled as a quantitative 'novelty bonus' that enhances the reward value of a novel option (Wittmann et al. 2008; Kakade & Dayan 2002). Whilst this may be essential for guiding normal exploratory behaviours, aberrantly high valuation of novelty is also associated with significant personal harm, including greater risk of substance abuse (Wills et al. 1994). Critically, variability in this novelty bonus may act as a quantitative index of poor, novelty-biased decision-making. For instance, heightened valuation of stimulus novelty is observed in patients with Parkinson's Disease who exhibit impulsive and compulsive behaviours in response to dopaminergic therapy (Djamshidian et al. 2011).

Heightened novelty seeking personality traits are also observed in ADHD (Downey et al. 1997; Lynn et al. 2005; Jacob et al. 2014), and ADHD (LaHoste et al. 1996; Rowe et al. 1998; Smalley et al. 1998; Faraone et al. 1999; Faraone et al. 2001; Barr et al. 2000; Eisenberg et al. 2000) and novelty seeking (Kluger et al. 2002; Munafò et al. 2008; Roussos et al. 2009; Ekelund et al. 1999; Tomitaka et al. 1999; Strobel et al. 1999; Okuyama et al. 2000; Ebstein et al. 1996) both appear to share genetic correlates in D4 receptor gene polymorphisms. However, to date no work has examined how increased novelty seeking impacts reward learning in the disorder.

1.3.6.4 Altered phasic prediction error and novelty signals in ADHD

By applying TD models to a reinforcement-learning task Chapter 5 also attempts to resolve several conflicting accounts of dopaminergic abnormalities in ADHD. ADHD is typically characterized as a hypodopaminergic disorder. However, several theoretical accounts suggest a more nuanced view. In disagreement with theories suggesting a completely blunted dopamine response (Volkow et al. 2005; Sagvolden et al. 2005), several findings have suggested that whilst tonic dopamine levels are reduced in the disorder, heightened phasic dopamine release is actually increased (Grace 2001; Seeman & Madras 2002; Badgaiyan et al. 2015). This is also in line with simulations suggesting that reward dysfunction in ADHD may be characterized by asymmetric positive and negative prediction error signals. Specifically, positive prediction error signals which are underpinned by phasic dopamine responses are expected to be heightened compared to negative prediction error signals (which may instead be mediated by inhibitory D2 receptors) (Cox et al. 2015). Clarification of these issues is central to developing accurate theoretical accounts of dopaminergic reward dysfunction in ADHD. As both prediction error and novelty signals are tightly coupled to phasic dopamine release, modelling these responses in blood oxygen level dependent (BOLD) (Ogawa et al. 1990) responses affords an indirect assessment of these hypotheses.

1.3.7 Motivation in ADHD

Another increasingly central component of dopaminergic reward dysfunction in ADHD is aberrant motivation. Incentive motivation, the process by which reward drives and

invigorates goal-directed behaviours, appears to be reduced in individuals with ADHD. Reductions in trait motivation in this disorder appear to be linked to lower D2/D3 receptor binding in the SN/VTA and ventral striatum (Volkow et al. 2011). In accordance with theories of ADHD positing reduced tonic dopamine, motivation to exert effort appears to be related to tonic dopamine levels (Niv et al. 2007). This lack of tonic motivational levels also appears to manifest as a heightened sensitivity to reward, with increasing motivational incentives improving performance on effortful tasks in ADHD (Fosco et al. 2015). Deficits in ostensibly higher order functions in ADHD may therefore be mediated at least in part by motivation. Indeed striatal dopamine appears to have a direct influence on cognitive flexibility (Aarts et al. 2010).

1.4 Acute and long term effects of methylphenidate on dopaminergic reward system

1.4.1 Acute effects on neuropsychology and neurobiology

As noted previously, stimulant medication appears to ameliorate executive functional deficits in ADHD (Barnett et al. 2001; Mehta et al. 2004; Ni et al. 2013; Aron et al. 2003; DeVito et al. 2009) and related network abnormalities in ADHD (Liddle et al. 2011). However, methylphenidate also appears to have similar effects on executive functions in controls (Mehta et al. 2000). This has led to speculation as to the lack of specificity of stimulant medication in treating ADHD, and even the validity of ADHD as a diagnosis. However, a different picture emerges when looking at reward function. For example, risky decision making is improved by methylphenidate in ADHD (DeVito et al. 2008a), but actually appears to be worsened in controls (Campbell-Meiklejohn et al. 2012). One possibility is that although methylphenidate may have similar actions on higher order functions that are not considered to rely primarily on dopaminergic function, it has different effects on reward and motivational processes directly linked to dopaminergic activity. Whilst stimulant medication may thus have a therapeutic effect by rebalancing abnormal dopaminergic activity in ADHD, these drugs may actually impair normal dopaminergic signaling. This is supported by findings methylphenidate has a greater therapeutic effect on reversal learning in more impulsive subjects

(Clatworthy et al. 2009). Similarly, other dopaminergic drugs appear to have distinct effects on reward learning in Parkinson's Disease (Rutledge et al. 2009) compared to healthy subjects (Pizzagalli et al. 2008). Chapters 4 and 5 address these potentially differential effects of stimulant medication on a) waiting impulsivity and b) reinforcement learning in ADHD and healthy controls.

1.4.2 Long term neurobiological effects of stimulant medication

Though long term benefits in broad outcome measures such as academic, social and occupational function are clear (Shaw et al. 2012), the exact effects of long term stimulant treatment in humans in ADHD are relatively poorly understood. However, a variety of behavioural and neurobiological changes have been observed in animal models. For instance, increased plasticity (Dommett et al. 2008), dendritic spine formation (Kim et al. 2009) and heightened expression of growth factors (Roeding et al. 2014; Simchon-Tenenbaum et al. 2015; Amiri et al. 2013) in mesolimbic circuitry have been reported. In humans reduced DAT binding potentials after long term methyphenidate treatment have been observed, and largely interpreted as an effect of tolerance (Wang et al. 2013). Human imaging studies have also suggested that grey matter volumes may be normalised by stimulant medication to some degree (Nakao et al. 2011; Spencer et al. 2013). This thesis addresses the long term effects of stimulant medication on a) striatal volume, b) SN/VTA microstructure, and c) computation of stimulus novelty.

2 Methods

The following methods chapter gives an overview of recruitment, and overall study design. Specific details of tasks, data processing and analysis are nested within each experimental chapter.

2.1 Participants

Patients with ADHD were recruited from specialist ADHD clinics at Sussex Partnership NHS Foundation Trust (SPFT). All had a DSM-IV confirmed diagnosis of ADHD and had been managed on a stable regimen of methylphenidate (minimum 18mg) or dexamfetamine (mimimum 10mg) for at least 2 months prior to study enrolment. Patients were sent letters detailing the study or approached at clinic and offered study information sheets if they were interested in participating in research. Participant diagnoses were performed by psychiatrists within SPTF clinics, assisted by the self-report long form of the Connor's Adult ADHD Rating Scale (CAARS) (Conners et al. 1999) and had therefore been exposed to materials used for rating ADHD symptoms within the study before. Control participants were recruited via community and classified advertising websites, as well as the University of Brighton mailing lists. Individuals who responded were screened over the telephone to ensure that they fully met the study criteria.

Participants were excluded in the case of psychotic symptomatology, learning difficulties, anxiety or depressive disorders not currently in remission, any neurological disorder, active drug or alcohol abuse, significant physical disability, suspected diminished capacity to consent, significant impairment of vision, hearing, or language comprehension, or if they were pregnant or aged <18 or >65. Individuals with a prior history of severe head injury, or metallic objects in the body deemed unsafe for MRI scanning were also excluded from the study. Control participants were also excluded for having any known hypersensitivity to methylphenidate, glaucoma, history of seizures, tinnitus, family history of tinnitus, motor tics, family history of Tourette's syndrome, serious cardiovascular conditions, current or recent use of monoamine oxidase inhibitors or current use of coumarin anticoagulants, anticonvulsants or antipsychotics. Due to the high prevalence of substance abuse in ADHD populations, both ADHD and control groups were asked during screening whether they had current history of substance abuse to ensure that they were not enrolled in the study. Psychiatrists recommending patients to the study were also aware of this criteria to

assist in screening patients. Participants were reimbursed £22.50 per session. In addition, participants could earn up to an additional £5 per session based on their performance in the novelty task.

Participants gave written, informed consent following full explanation of the experimental procedures. Local and national ethical approvals were obtained from Brighton and Sussex Medical School Research Governance and Ethics Committee (14/014/HAR; 12/131/HAR) and the East of England (Hertfordshire) National Research Ethics Committee (reference: 12/EE/0256).

2.2 Study design

A repeated-measures randomized, placebo controlled study design was utilized in which all participants attended two experimental sessions separated by a minimum of 1 week. ADHD patients were asked to abstain from their regular ADHD medication for the test day and 2 days prior to testing. At the start of the first session participants were randomized to receive either stimulant medication or placebo. The alternate treatment was given on the second experimental session. ADHD participants were blindly administered either their normal morning medication dose or placebo. Control participants received either 20mg of methylphenidate or placebo. Control methylphenidate dose was based on the average daily dose in the ADHD group assuming the average 2.5 times daily dosing. All medication was concealed in an opaque, easily absorbed capsule to ensure both participant and researcher were blind to treatment. A consultant psychiatrist was aware of treatment allocation to ensure safety, though played no role in face-to-face participant testing.

2.3 Procedure

Participants arrived on their testing day and were given an opportunity to ask questions about the study before signing consent forms. Patients with ADHD were asked to bring their usual daily medication with them after two days of abstinence. Upon arrival this was taken from them for later dosing. On the first session, participants were then given the Connor's Adult ADHD Rating Scale (CAARS; Self Report, Long form), Becks Depression Inventory (BDI), and the State and Trait Anxiety Index (STAI) to fill out, before being blindly administered either drug or placebo masked in a gelatine

capsule. Immediately afterwards participants underwent two pre-task 'familiarisation' procedures for the 3-armed bandit (reinforcement learning and novelty; See Chapter 5 for details) task which was to be performed later in the MRI scanner. Participants were then administered the Tridimensional Personality Questionnaire (TPQ) and the National Adult Reading Test (NART).

One hour after dosing, participants were given a thorough explanation of the 3-armed bandit task, and assessed and prepared for the scanning environment. After the research and radiography teams were satisfied that the participant met all safety criteria, they were laid supine on the scanner bed with extra padding to reduce movement where necessary and given a demonstration of the button box used for task responses before scanning commenced. Each scanning session consisted of a standard functional EPI sequence during the 3-armed bandit task (spread over three individual runs) and a multi-echo functional EPI during rest, as well as a series of structural and diffusion imaging sequences that were collected over the course of the two sessions (Table 2.1). Scanning was timed so that participants performed the 3-armed bandit task 90 minutes after dosing to ensure peak brain concentration had been reached (Volkow et al. 1998). Following this, the participants underwent a series of behavioural tasks, including the 5-choice serial reaction time task (5-CSRTT). The 5-CSRTT data were analysed as part of this thesis and are discussed in more detail in Chapter 4. Data from the other behavioural tasks are not reported as part of this work.

During the second visit, participants underwent the same procedure and administered the capsule they had not taken on the previous session. An alternate set of stimuli was used for the 3-armed bandit task and prefamiliarisation sessions on the second session. They then completed the Multidimensional Personality Questionnaire (MPQ) before the scan. After scanning, participants completed scans and behavioural tasks as before. Participants were assessed for safety and debriefed. Additionally, patients with ADHD were interviewed to assess the length of their treatment prior to the study, as well as their medication and dosage history.

To combat fatigue with the length of the session participants were offered breaks between tasks as necessary. Retention rate was still relatively high, even within the ADHD group, with the final task being completed by 28 controls and 25 patients. It should also be noted that this attrition rate was not solely attributable to fatigue (e.g. several participants arrived late for and experimental sessions had to be cut short).

Table 2.1 Study protocol and timing

Dose time	Session 1	Dose time	Session 2
-00:20	Arrival	-00:20	Arrival
-00:20	Consent & safety check	-00:20	Safety check
-00:10	CAARS, BDI, STAI		
00:00	Dose	00:00	Dose
00:00	Stimuli familiarisation (passive)	00:00	Stimuli familiarisation (passive)
00:05	Stimuli familiarisation (active)	00:05	Stimuli familiarisation (active)
00:15	TPQ	00:15	MPQ
00:50	Task instruction	00:50	Task instruction
1:00	Enter scanner	1:00	Enter scanner
1:10	MT-MRI (and task practice)	1:10	MPRAGE (and task practice)
		1:18	Diffusion MRI
1:30	Task based functional EPI	1:30	Task based functional EPI
2:05	Resting state multi-echo EPI	2:05	Resting state multi-echo EPI
2:15	Exit scanner	2:15	Exit scanner
2:20	Exploration/Exploitation task	2:20	Exploration/Exploitation task
2:50	Model-based/Model-free task	2:50	Model-based/Model free-task
3:15	Impulsivity task	3:15	Impulsivity task
3:45	Debriefing	3:45	Debriefing

2.4 Materials

The long-form self report version of the CAARS was used to assess ADHD symptom severity (Conners et al. 1999). This consists of 8 clinical scales, and consists of 66 Likert items and is separable into 8 subscales: Inattentive/Memory problems, Hyperactivity/Restlessness, Impulsivity/Emotional Lability, Problems with Self-Concept, DSM IV Inattentive Symptoms, DSM IV Hyperactive-Impulsive Symptoms, Total DSM IV ADHD symptoms and the CAARS total ADHD Index. An inconsistency scale can additionally be derived to determine inconsistent reporting. However, this was not used in the present study due to each participant having a psychiatrist confirmed diagnosis of ADHD. The BDI is a 21-question self-report Likert scale assessing the severity of depression including both affective and physical components of the disorder (Beck et al. 1996). The STAI is a 40 question inventory of 40 self-report Likert items about anxiety affect that is divisible into two 20 item scales pertaining to trait anxiety 'How you feel generally' and state anxiety 'How you feel right now' (Spielberger 1983). The TPQ consists of 100 true-false questions measures originally measuring three factors: novelty seeking, harm avoidance and reward dependence each with four subscales (Cloninger et al. 1991). Of particular interest to this study, is the persistence subscale of reward dependence due to its questions probing motivation e.g. 'I usually push myself harder than most people do because I want to do as well as I possibly can.' The MPQ contains 276 true-false items across 3 broad factors (Positive Emotionality, Negative Emotionality and Contraint) and 11 primary trait dimensions (Tellegen & Waller 2008). Of particular interest is the trait dimension of Achievement (consisting of items such as 'I welcome difficult and demanding tasks') which has been used in previous studies to measure trait motivation in adult ADHD (Volkow et al. 2011).

2.5 Imaging

All imaging was performed on a 1.5T MRI scanner ((Siemens Magnetom Avanto, Siemens, Erlangen, Germany), with a maximum gradient strength of 44 mTm^{-1} and a 32-channel head coil for signal reception.

2.5.1 Diffusion MRI

For diffusion MR imaging a multi-slice twice refocused spin echo echo-planar imaging (EPI) acquisition was used, with 60 contiguous near axial slices acquired with 2.5mm^3 isotropic voxels. Acquisition had a TE of 86ms, and a TR of 7.7s. A maximum diffusion weighting of b=1500 smm^{-2} was applied. 60 diffusion-weighted brain volumes with diffusion gradients uniformly distributed in space were collected at each slice location, as well as 7 volumes without diffusion weighting applied. The number of diffusion directions (60) were collected in order to allow for the High Angular Resolution Diffusion Imaging (HARDI) approach adopted in Chapter 4 so as to be able to successfully resolve crossing fibre configurations (with a minimum of 45 recommended HARDI) (Tournier et al. 2013). Although a higher b value has also been recommended (Tournier et al. 2013), at 1.5T it was deemed the loss of SNR would not be worthwhile.

2.5.2 FLASH 3D

A multi-parameter protocol adapted from a 3D multi-echo fast low angle shot (FLASH) sequence was used to calculate MT saturation maps (Weiskopf & Helms 2008). Three co-localised 3D multi-echo flash sequences were acquired in the sagittal plane. Proton density weighted volumes were acquired with a TR of 24, a TE from 2.51 to 21.9ms (eight equidistant bipolar echoes collected), and flip angle (α) of 6°, with 1.25mm^3 resolution (FOV: 240x217.5mm^2, 144 partitions). T1 weighted volumes were acquired with a TR of 19, a TE ranging from 2.51 to 10.82ms (four equidistant bipolar echoes collected), and a flip angle of 20°, with 1.25mm^3 resolution (FOV: 240x217.5mm^2, 144 partitions). MT weighted volumes were acquired at a TR of 30, with a TE ranging from 2.51 to 10.82ms, a flip angle of 12°, with magnetisation transfer contrast on, and 1.25x1x1mm resolution. Calculation and optimisation of MT saturation maps and acquisition is discussed in Chapter 3.

2.5.3 MPRAGE

Standard T1 weighted volumes for VBM are acquired with a magnetization-prepared rapid gradient echo sequence (MPRAGE) (Mugler & Brookeman 1990) along the axial plane with an isotropic voxel resolution of $1mm^3$ (FOV: $256x240mm^2$, 192 partitions), with a TR of 27.3 ms, TE of 3.57ms and a flip angle of 7°.

2.5.4 Task-based fMRI

T2*-weighted echo planar images (EPIs) were acquired on a 1.5T Siemens Avanto MR scanner equipped with a 32 channel head-coil using a -30° tilted acquisition to reduce orbitofrontal dropout (Deichmann et al. 2003). Each volume provided whole brain coverage (34 interleaved ascending 3mm axial slices with 1mm inter-slice gap, echo-time 43msec: TR 2.52s, in-plane resolution 3mm).

2.5.5 Multi-echo resting state EPI

Resting-state functional images were collected with a multi-echo EPI sequence (Poser et al. 2006) with a FOV of 240x240mm and 31 axial slices. Slice thickness was 4.2mm, with an in plane resolution of $3.8mm^2$. Acquisition occurs with a TR 2.57s, and flip angle of 90°. TEs are at 15, 34, and 54ms. Although these data were not analysed for this thesis, they were acquired within this overarching study so are here for completeness.

2.6 Demographics

Demographic and behavioural data for ADHD and control participants are summarized in Table 2.2.Groups were matched for age (ADHD: 33.7(±1.7) years, controls: 32.6(±1.7)) years, $F_{(1,58)}$=0.20, p=0.66), IQ (ADHD: 109.0±1.2, controls: 110.1±1.3, $F_{(1,58)}$=0.40, p=0.53), gender and handedness. The ADHD group scored significantly higher on all CAARS subscales. ADHD participants had significantly higher scores on the BDI (ADHD=13.7 (±0.9), controls = 5.6 (±1.2), $F_{(1,58)}$=17.01, p<0.001) and STAI trait anxiety (Trait: ADHD=53.5 (±2.0), controls=36.5 (±2.0), $F_{(1,58)}$= 36.51, p<0.001).

Table 2.2 Participant demographics

Measure	Mean scores (SE)		F	p
	ADHD	Controls		
N	30	30	---	---
Male	19	19	---	---
Female	11	11	---	---
Age	33.7 (1.74)	32.6 (1.2)	0.20	0.66
Handedness				
Right-dominant	28	29	---	---
Left-dominant	1	1	---	---
Ambidextrous	1	0	---	---
FSIQ[1]	109.0 (1.2)	110.1 (1.3)	0.40	0.53
CAARS ADHD Index	24.0 (1.0)	8.6 (0.9)	133.21	<.001
Attention/Memory problems	26.7 (1.0)	9.9 (1.0)	123.48	<.001
Hyperactivity/Motor restlessness	24.4 (1.2)	11.3 (1.0)	68.81	<.001
Impulsivity/Emotional lability	23.7 (1.3)	7.6 (0.8)	109.13	<.001
Problems with self-concept	11.3 (0.9)	5.6 (0.8)	22.50	<.001
DSM Total ADHD score	37.6 (1.6)	11.8 (1.3)	159.66	<.001
DSM Inattention	19.3 (0.8)	7.0 (0.8)	125.28	<.001
DSM Hyperactivity & Impulsivity	18.3 (1.0)	5.7 (0.7)	110.44	<.001

[1] As estimated by National Adult Reading Test (NART) scores

2.6.1 Medication

Twenty-eight ADHD participants were treated with methylphenidate and two with dexamphetamine. Within those taking methylphenidate, a variety of different regimens were observed (Figure 2.1). Several ADHD and control participants were also taking SSRI or SNRI antidepressant. Fischer's Exact Test (FET) detected no significant different between the groups (ADHD = 6, Controls = 1, p = .103). In order to calculate approximate equivalent doses between methylphenidate and dexamfetamine, dexamfetamine doses were doubled. This is supported by various studies performing comparative analysis of the two drugs (for a review, see (Arnold 2000)), as well as the maximum recommended dose according to NICE guidelines. The mean methylphenidate dose in mg for the ADHD group was 50 ± 21.0. Excluding participants currently taking dexamfetamine, daily methylphenidate dose in mg was 49.7 ± 21.7.

Immediate release methylphenidate dose for controls was matched to the daily doses observed in the ADHD group. The equivalent immediate release dose for the ADHD group was therefore calculated based on mean daily dose, to account for differences in drug formulation and release schedule. The NICE recommendation of an immediate-release methylphenidate dose schedule of 1-4 times (mean 2.5), therefore indicates a 20mg equivalent acute dose. As such, 20mg of immediate-release methylphenidate was administered to controls.

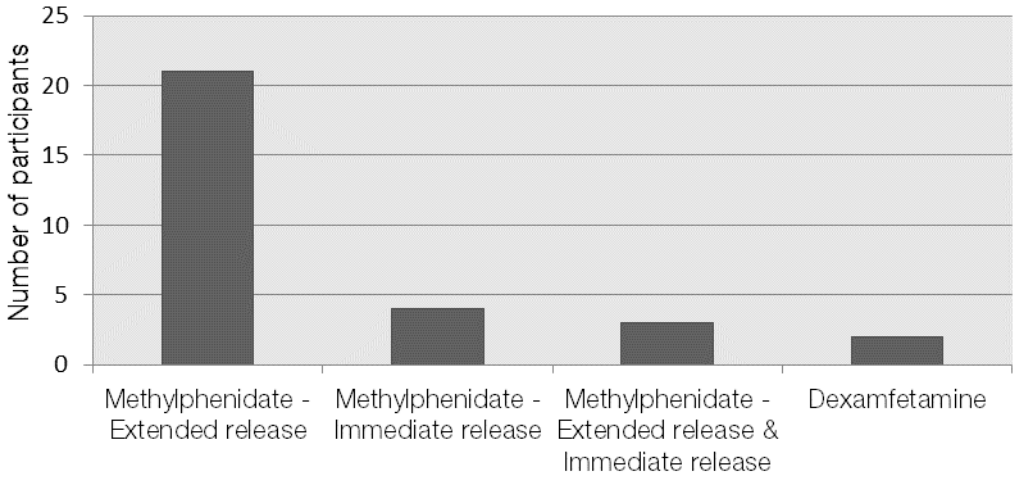

Figure 2.1 Distribution of medication regimens in the ADHD group

3 Detection of persistent striatal abnormalities in adult ADHD using MT saturation but not T1 weighted VBM

Attention Deficit Hyperactivity Disorder (ADHD) in childhood has been robustly linked to striatal volumetric abnormalities. By contrast, such differences have been less frequently detected in adult population voxel-based morphometry (VBM) studies. This has been suggested to reflect maturation- and treatment-related normalisation of striatal morphometry. The absence of striatal volumetric reductions in adult ADHD would also suggest that whilst abnormal striatal volumes are central to childhood ADHD, they do not necessarily explain the persistence of these symptoms in adulthood. However, several contradictory findings suggest that striatal morphological abnormalities may not remit over time. Instead, the lack of voxel-wise whole-brain corrected evidence implicating the striatum in adult ADHD may reflect the poor sensitivity of T1 weighted images to detecting subcortical changes. To address this, I performed VBM of both magnetisation transfer (MT) saturation maps optimised for subcortical contrast and T1 weighted images in 30 patients with ADHD and 30 age, IQ, gender and handedness matched controls. In ADHD, volumetric reductions within the left ventral striatum were observed using MT saturation VBM. Identically pre-processed VBM analyses of T1 weighted images in the same subjects were however insensitive to these differences. By contrast, both techniques report similar abnormalities in the right inferior parietal cortex. Finally, I show that differences in striatal iron content may explain the reduced sensitivity of T1-weighted images to detecting striatal volumetric differences in adult ADHD. These results suggest that prior VBM studies reporting an absence of differences in the striatum in adult ADHD reflects methodological insensitivity of T1 weighted VBM to these changes, and that striatal abnormalities in ADHD persist into adulthood.

3.1 Introduction

As discussed, the striatum has been a central focus of ADHD research. Morphometric studies have offered a non-invasive and easily replicable method for indexing striatal abnormalities in childhood ADHD. VBM results have confirmed the significance of these even in assumption free analyses without *a priori* regions of interest and using stringent criteria for whole brain statistical correction. These results have been less consistent in adulthood however, and whilst large scale meta-analyses have confirmed the importance of altered striatal morphology in childhood ADHD these reports have not supported the presence of these abnormalities in adulthood (Frodl & Skokauskas 2012). Such findings have suggested that this may be due to a normalisation of striatal volumes with age and long term treatment (Nakao et al. 2011). The absence of striatal differences in these symptomatic adult ADHD samples would also however suggest that ongoing abnormalities in striatal morphology are not required for the persistence of symptoms.

Other methodological explanations could however account for the absence of whole-brain corrected results implicating the striatum in adult ADHD. Indeed, less statistically stringent ROI based approaches have detected striatal changes in adult ADHD samples where whole-brain statistical correction were not met (Almeida Montes et al. 2010; Seidman et al. 2011). Importantly, large prospective VBM investigations have also suggested that striatal abnormalities are observed in adult ADHD when followed up from childhood (Proal et al. 2011). Interestingly, in this prospective dataset no effects of medication on these striatal differences were detected.

A currently unexplored reason for explaining these apparently contradictory findings may be poor methodological sensitivity. Not only have meta-analyses had smaller samples of adult studies to draw on, but T1 weighted volumes that are typically used in these VBM studies have poor subcortical contrast, and subsequently produce less accurate automated segmentations. Specifically, the complex white matter pathways entwined within subcortical structures mean that grey and white matter boundaries are less well defined (Helms et al. 2009). Moreover, the high levels of brain iron in these regions is well demonstrated to shorted T1 thus reducing image contrast (Helms et al. 2009). Problematically, subcortical segmentation accuracy using T1-weighted images may actually also worsen with age; striatal iron is well documented to accumulate over the lifespan (Martin et al. 1998). This would therefore be predicted to reduce

segmentation accuracy in older participants. Recent evidence has also suggested that ADHD (Cortese et al. 2012; Adisetiyo et al. 2014), and possibly its treatment (Adisetiyo et al. 2014), are also associated with altered brain iron levels. Previous investigations using T1 weighted images to examine the impact of ADHD status, medication and maturation on striatal volumes may therefore have been systematically biased by these factors. Improving methodological accuracy and sensitivity in VBM analyses is therefore essential to examine whether striatal volumetric differences associated with ADHD do indeed ameliorate with maturation and stimulant treatment, or if the absence of striatal findings in adulthood rather reflects other confounding factors.

MT saturation maps derived from a multi-echo fast angle low shot (FLASH) 3D multi-parameter protocols have exquisite subcortical contrast, providing superior automatic segmentation to T1 weighted images traditionally used in VBM (Helms et al. 2009). Due to the sensitivity to macromolecular proteins such as myelin, MT saturation maps allow more accurate delineation of the complex white patter pathways within the striatum and other subcortical regions. Importantly, MT saturation maps are also not affected by the T1 shortening effects of iron highly concentrated in the basal ganglia (Helms, Dathe, Kallenberg, et al. 2008). I therefore sought to leverage this improved anatomical accuracy to offer a more definitive examination of any structural changes associated with ADHD in adulthood. As well as attempting to reconcile some of the inconsistencies in the ADHD literature, I also sought to compare the sensitivity of MT saturation with T1 maps to structural differences in the same group of participants.

This work therefore employs VBM of MT saturation maps in 30 adults with ADHD and 30 age-, IQ- and gender-matched controls. To specifically assess any enhancements in sensitivity proffered by this approach, I compare these results to a typical VBM analysis of T1 weighted images in the same subjects.

3.2 Methods

3.2.1 MT background

3.2.1.1 The basis of MT contrast

Protons bound to macromolecules such as large proteins, myelin and cell membranes are not detectable by typical MR sequences, due to their restricted range of movement resulting in the MR signal decaying more rapidly (~tens of microseconds) than is measurable using typical echo times (~milliseconds). Such sequences are therefore restricted to measurement of 'free' protons in liquids that are highly mobile, and have longer signal decay times. However, as these free protons are in constant motion, they frequently come into contact with macromolecular proteins, where protons may exchange between the free and macromolecular pools. MT imaging exploits this interactive magnetisation exchange that occurs either by direct exchange of the hydrogen atom or spin-spin interactions to quantify macromolecular presence (Henkelman et al. 2001).

Proton T2 is reflected in the width of the resonance line in the MR spectrum. Mobile protons with a long T2 have a narrow resonance line around the L'armor frequency (the frequency at which proton magnetic moments precess in the magnetic field). By contrast, macromolecular protons with a short T2 have a broad resonance line (Figure 3.1). By using an RF pulse with a frequency that is distant from the central narrow resonance line ('off-resonance') that is characterised by long T2/mobile protons, it is possible to selectively excite macromolecular protons without affecting the liquid ones (Figure 3.2). With sufficient off-resonance power applied, macromolecular spins reach a state of saturation, where up and down spins are equalised and net magnetisation vector reaches zero. If this magnetisation is partially transferred to the liquid protons via magnetization exchange, they can become partially saturated, resulting in reduced signal intensity. This signal attenuation in regions where fluid and macromolecular protons are in contact forms the basis of MT contrast.

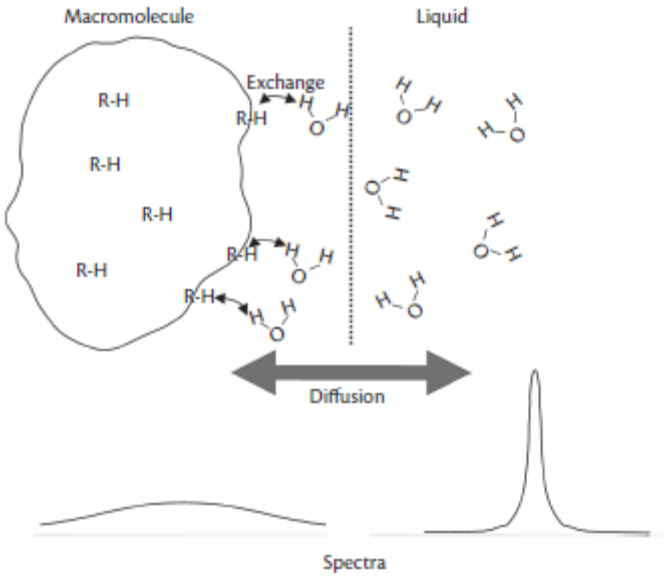

Figure 3.1 Magnetisation exchange between macromolecular and liquid protons. Reproduced from (Horsfield & Cercignani 2015).

A macromolecule with functional groups (R) with bonded hydrogen (H) atoms that are available to exchange with those in water. Hydrogen atoms within macromolecules are relatively immobile, thus exhibiting a short T2 not normally detectable on an MR image and a broad resonance line in the MR spectrum. Hydrogen atoms within liquids move freely, have a long T2 and a narrow line of resonance. Spin states of macromolecular and mobile protons are in exchange, so the magnetisation within the macromolecule has an effect on those in fluid.

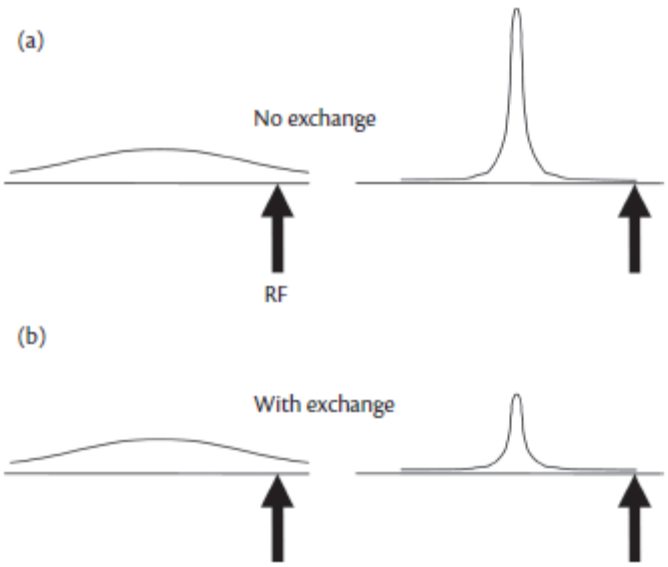

Figure 3.2 Effects on magnetisation exchange on signal MR signal amplitude. Reproduced from (Horsfield & Cercignani 2015).

An off resonance frequency pulse will only directly excite bound molecular protons, and not those in fluid. However, if there is magnetisation is transferred to the fluid the signal amplitude is reduced (b), resulting in reduced signal in voxels where fluid is in contact with macromolecules.

3.2.1.2 MT saturation

This chapter employs measures of MT saturation with the specific goal of maximising subcortical contrast. Whilst other approaches have a greater ability to quantitatively index macromolecular proton properties, this is coupled with a higher level of model complexity and greater scan times needed for robust parameter estimation (Levesque & Pike 2009). Here I instead apply a simplified model of MT saturation developed by Helms et al which requires measurement of just three parameters (Helms, Dathe, Kallenberg, et al. 2008) using an adapted multi-parameter FLASH-3D protocol, and can be used to derive MT saturation maps with excellent subcortical contrast (Helms et al. 2009). Specifically, 3 volumes are acquired. The first 2, without MT saturation, are proton density- (S_{PD}) and T1-weighted (S_{T1}), respectively. If small flip angles (**α)** are used, and TRs are much shorter than the T_1 of tissue, the signal equation for a FLASH sequence can be approximated as

$$S = A\alpha \frac{TR/T_1}{\alpha^2/2 + TR/T_1} \qquad \text{[Eq 3.1]}$$

By combining S_{PD} and S_{T1} and using Eq 3.1 it is possible to estimate *A* (the amplitude of the echo at TE) and T_1 (Helms, Dathe & Dechent 2008).

For the third volume, which is MT-weighted, Helms et al (Helms, Dathe & Dechent 2008) showed that the signal can be approximated by

$$S_{MT} = A\alpha \frac{TR/T_1}{\alpha^2/2 + \delta + TR/T_1}, \qquad \text{[Eq 3.2]}$$

Where δ is the MT saturation, which can be calculated with knowledge of A and T_1.

MT saturation derived from such protocols have been shown to be sensitive to myelin changes (Draganski et al. 2011), and offer superior contrast in subcortical regions to T1 weighted images (Helms et al. 2009). Due to the nature of these maps, they are also inherently corrected for B0 field inhomogeneities and T1 effects (Helms, Dathe, Kallenberg, et al. 2008). Importantly, for the purposes of the present study, this excludes bias resulting from the T1 shortening effects of iron.

3.2.2 MT Optimisation

To optimise the MT sequence used for the study, I sought to select the best combination of acquisition parameters within acceptable times to maximize the contrast-to-noise ratio (CNR) between the SN/VTA and the surrounding white matter. This was specifically performed on the SN/VTA to improve anatomical accuracy in manual tracing for the parcellation analyses in Chapter 4, but also assuming that the acquisition parameters derived would improve the contrast between all the subcortical structures and the neighbouring white matter.

3.2.2.1 Theory

Based on Eq 3.2, it is possible to estimate the MT saturation, δ as:

$$\delta = \left(A\alpha/S_{MT} - 1\right) R_1 TR - \alpha^2/2 \qquad \text{[Eq 3.3]}$$

Where R1: inverse of T_1. Contrast, C, on the MT saturation images, can therefore be defined as the difference between the MT saturation value in the substantia nigra (δ_{SN}) and in the white matter (δ_{WM}). As differing acquisition parameters also affect the signal-to-noise ratio (SNR) of the δ maps, and the CNR is affected by the SNR, the propagation of error equation (Bevington 1969) was used to estimate the variance of the signal in δ maps, relative to the variance of S_{MT} (MT signal):

$$var(\delta) = \frac{\partial \delta}{\partial S_{MT}} = \frac{A\alpha R_1 TR}{S_{MT}^2} \qquad \text{[Eq 3.4]}$$

With knowledge of the quantitative MT parameters of the anatomical areas of interest, it is possible to use Sled and Pike's model of MT (Sled & Pike 2000) signal to simulate S_{MT} in both, eq 3.1 and 3.2. This model expresses the expected signal in a MT-saturated acquisition as a function of both, intrinsic tissue parameters regulating relaxometry and MT exchange, and acquisition parameters such as the amount of MT saturation. The contrast-to-noise ratio (CNR) can then be estimated as:

$$CNR = \frac{\delta_{WM} - \delta_{SN}}{1/2\sqrt{var(\delta_{SN}) - var(\delta_{WM})}} \qquad \text{[Eq 3.5]}$$

3.2.2.2 Simulations

The quantitative MT parameters (R_1, T_{2f}, T_{2r}, k_f, F) in Sled and Pike's model were calculated from full qMT datasets obtained from 5 healthy subjects. First, the substantia nigra and cerebral peduncles were manually outlined on proton-density weighted images to avoid bias (Figure 3.3). S_{MT} was then calculated for the substantia nigra and cerebral peduncles (left and right pooled, averaged across subjects) as a function of MT saturation power and offset frequency. This expression was then incorporated into eqs 3.1 and 3.2, and thus eq 3.3. The maximum CNR value was then estimated by searching the parameter space using the following parameter ranges: TR: 20-30ms; α: 3° to 15°; MT pulse power (ω): 200 to 900 rad/s; MT pulse offset frequency (Δ): 1 to 5 kHz. This generated optimal acquisition values, i.e. the values of of TR, α, ω and Δ that maximises the CNR for the substantia nigra.

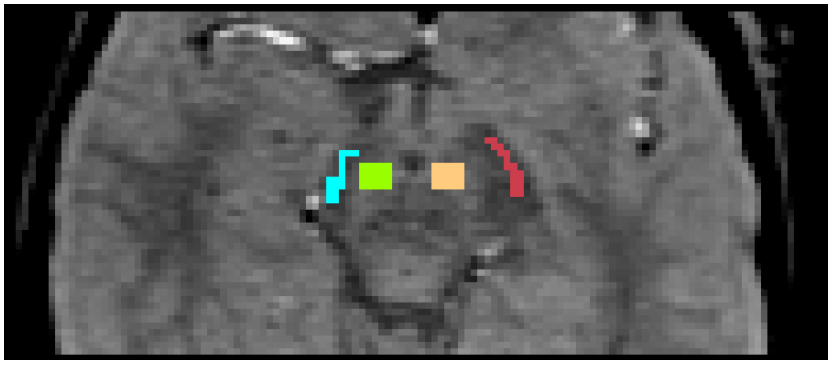

Figure 3.3 ROIs for qMT parameter estimates.

Estimates of qMT parameters were taken from ROIs (left and right substantia nigra, left and right cerebral peduncles) manually outlined on proton density scans (blue=left peduncle, red=right peduncle, green=left SN, orange=right SN)

3.2.2.3 Testing simulation predictions

To test whether the predictions from these simulations resulted in improved data from the MT sequence, I compared the optimal MT sequence against two sub-optimal sequences, all acquired from the same healthy participant (male, 24 years old). From this participant three MT-weighted 3D FLASH sequences (4 echoes, TEs ranging from 2.51 to 10.82 ms) were collected with 3 different combinations of TR, α, ω, and Δ

based on the results of the simulations. The optimal acquisition had a TR of 30ms, α of 12°, ω of 900 rad/s, Δ of 1kHz. The first suboptimal acquisition had a TR of 24ms, an α of 6°, ω of 900 rad/s, Δ of 1kHz, and the second suboptimal acquisition had a TR of 30ms, an α of 12°, ω of 300 rad/s, Δ of 1kHz. In addition to this one proton-density weighted multi-echo 3D FLASH (4 echoes, same TEs as above, TR=24, α=6°) and a T1-weighted 3D FLASH (4 echoes, same TEs as above, TR=19 ms, α=6°) set were acquired.

In order to ascertain if the optimal acquisition improved the CNR in this sample, A, R_1 and δ maps for each of the MT sequences were calculated as described above (Helms et al. 2009). From these maps, ROIs were delineated (as above). S_{MT} values were obtained from these ROIs for each of the 3 δ maps (Figure 3.4), with the relative contrast estimated for each as $C_r=(\delta_{WM}-\delta_{SN})/(\delta_{WM}+\delta_{SN})$.

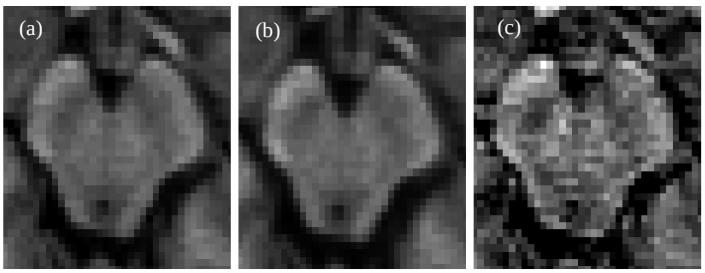

Figure 3.4 δ maps with differing acquisition parameters.
(a) shows the optimal acquisition, (b) shows suboptimal acquisition 1 and (c) shows suboptimal acquisition 2

C_r was 0.126 for the optimal acquisition, 0.088 for suboptimal acquisition 1, and 0.160 for suboptimal acquisition 2. Visual examination of the images revealed that suboptimal acquisition 2 was too noisy to be considered for further analysis (Figure 3.4c), despite having the highest C_r, reiterating the importance of optimising the CNR, instead of the contrast. Of the two usable scans, the C_r was highest for the optimal acquisition. To ascertain the impact this analysis had on segmentation of the substantia nigra, the VBM8 segmentation tool was used. Results show far clearer segmentation of the substantia nigra on the optimal acquisition (Figure 3.5).

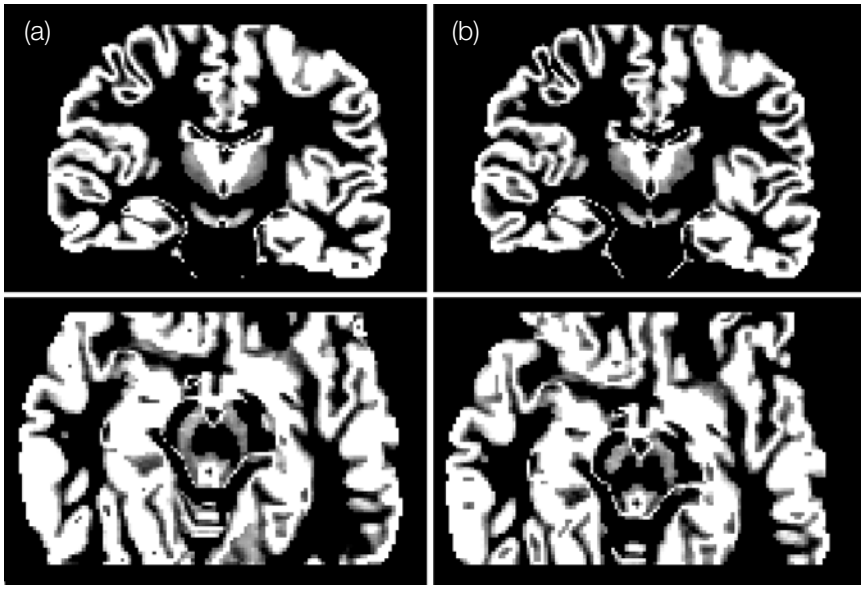

Figure 3.5 Segmentation of the substantia nigra after (a) Optimal acquisition (b) Suboptimal acquisition 1

3.2.3 VBM study methods

3.2.3.1 Participants

Data from all thirty patients with ADHD (mean 34 (±9.5) years; 19 male) and 30 controls (mean 33 (± 9.5) years; 19 male) were included in the analyses reported below. See Methods chapter (Chapter 2) for overall sample characteristics

3.2.3.2 Questionnaires

The CAARS (Conners et al. 1999) was used to index current ADHD symptom severity, and BDI (Beck et al. 1996) and STAI (Spielberger 1983) were used to assess depression and anxiety scores respectively.

3.2.3.3 Scanning

MT maps were calculated from a multi-parameter protocol adapted from a 3D FLASH sequence (Weiskopf & Helms 2008). Three co-localised 3D multi-echo flash

sequences were acquired in the sagittal plane, each with 1.25mm^3 resolution (FOV: 240x217.5mm^2, 144 partitions). Proton density weighted volumes were acquired with TR=24ms, TE from 2.51 to 21.9ms (eight equidistant bipolar echoes collected), and flip angle (α) of 6°. T1 weighted volumes were acquired at TR=19ms, TE ranging from 2.51 to 10.82ms (four equidistant bipolar echoes collected), and a flip angle of 20°. MT weighted volumes were acquired at TR=30ms, with the same 4 TEs as the T1-weighted volumes, a flip angle of 12°, and with magnetisation transfer contrast on. These parameters were selected to maximise the contrast between the white matter and the substantia nigra as described in the previous section. Standard T1 weighted volumes for VBM are acquired with a magnetization-prepared rapid gradient echo sequence (MPRAGE) (Mugler & Brookeman 1990) along the axial plane with an isotropic voxel resolution of 1mm^3 (FOV: 256x240mm^2, 192 partitions), with TR=27.3ms, TE=3.57ms and a flip angle of 7°.

3.2.3.4 Computation of MT saturation maps

The multiple echoes were averaged for each acquisition volume, and the resulting volumes were co-registered (with FLIRT, part of FS) using the T1-weighted image as a reference. The MT saturation, δ, was calculated voxelwise according to Eq 3.3, after deriving A and T1 as described by Helms et al. (Helms, Dathe, Kallenberg, et al. 2008). The resulting maps show a contrast similar to T1-weighted scans and can be entered directly into a VBM pipeline.

3.2.3.5 VBM preprocessing and analysis

MT saturation and T1 weighted maps were processed with identical pipeline. First, they were segmented using the VBM8 toolbox in SPM8 (http://www.fil.ion.ucl.ac.uk/spm/) and then smoothed with a 5mm^3 Gaussian kernel. Group comparisons were performed according to the General Linear Model (GLM), controlling for age, total intracranial volumes (derived separately for each modality), and BDI and STAI trait scores. Treatment effects within the ADHD group were examined in SPM using regression analyses, with length of time on medication (in months) as the variable of interest and age, total intracranial volume, BDI and STAI trait scores as covariates. Analyses were thresholded at $p < 0.001$ uncorrected, with surviving

clusters thresholded at $p < 0.05$ corrected for False Discovery Rate (FDR) at cluster level.

3.2.3.6 Iron content assessment

Densely packed ferric ions in ferritin cause local changes in magnetic susceptibility, with surrounding water molecules experiencing a higher magnetic field and shortening relaxation times of molecules diffusing through them. T2* images, which measure 'observed' transverse relaxation time, incorporate relaxation associated with such field inhomogeneities, in addition to the contributions of 'true' tissue relaxation reflecting spin spin interactions (ie T2), in addition to contributions from local magnetic field inhomogeneity. R2* (1/T2*) therefore gives the rate of relaxation associated with local field inhomogeneities, and has been shown to correspond highly to grey matter iron concentrations in post-mortem investigations (Langkammer et al. 2010).

Post-hoc assessment of iron content was therefore indexed in the left ventral striatum using R2* (=1/T2*) maps and a mask derived from Martinez et al. (Martinez et al. 2003). R2* Maps were obtained from the PD-density images acquired during the 3D flash sequence. As 8 echoes are acquired for this scans, R2* could be estimated by linear fitting of the equation ln(S(t)) = ln(S0) - tR2* to the 8 echo images. In the equation, S is the measured signal, S0 is the signal at the equilibrium, t is time at which the signal is sampled (corresponding to the 8 TEs) and R2* is the transverse relaxation rate to be estimated.

3.3 Results

3.3.1 MT saturation maps

Group average MT saturation map is shown alongside a corresponding T1 group average (Figure 3.6). The comparison clearly shows the augmented contrast in subcortical regions. The difference of averaged segmentations from each modality also shows clear enhancement in subcortical segmentation (Figure 3.6).

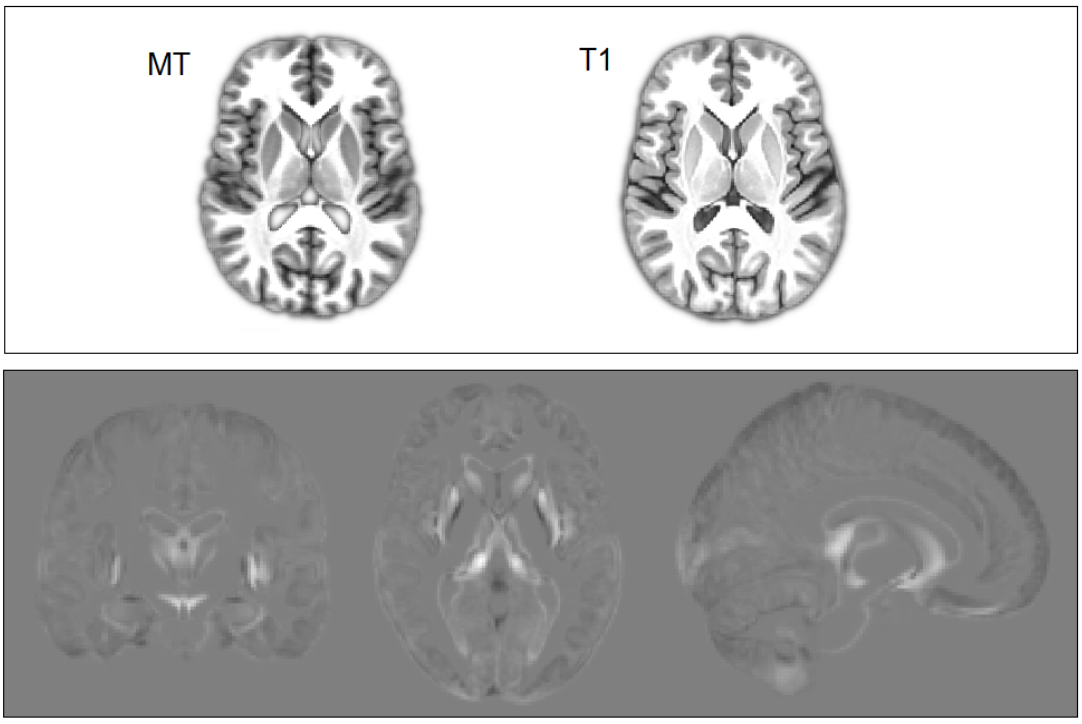

Figure 3.6 Comparison of group-averaged MT and T1 weighted volumes.

Top: Group averages of MT saturation compared to T1 show enhanced subcortical contrast. Bottom: Difference (MT-T1) in image intensity of segmented averaged maps showing enhanced contrast and segmentation in subcortical regions.

3.3.2 VBM results

MT saturation VBM revealed lower grey matter volumes in the left ventral striatum (*FDR* $p < 0.05$*)* and right inferior parietal lobe in ADHD compared to controls (*FDR* $p < 0.05$*)* (Figure 3.7; Figure 3.8; Table 3.1). By contrast, T1 weighted VBM reported the same abnormalities in the right inferior parietal lobe (albeit not reaching FDR cluster level significance), but did not reveal any volumetric alterations in striatal regions (Figure 3.8; Table 3.2). Neither modality detected statistically significant volumetric increases in the ADHD group compared to controls. Finally to test whether the length of time on medication indicated any normalisation or other changes in regional brain volumes within the ADHD group, I assessed negative and positive correlations between medication time and T1 and MT images. No statistically significant effects of medication were detected using T1 weighted or MT saturation VBM.

3.3.3 Iron alterations in the left ventral striatum

To examine whether abnormal iron content may contribute to the methodological insensitivity of T1 to the left hemispheric ventral striatal abnormalities reported, I used a ROI approach to assess R2* as an index for brain iron content. This revealed increased R2* in ADHD (14.20 ± 2.89) compared to controls (13.26 ± 1.56) in the left ventral striatum ($F(1, 54) = 5.60$, $p = 0.002$). Finally, I examined whether these iron differences in ADHD might be influenced by ageing or medication use. Left ventral striatal R2* correlated with age ($rho = 0.37$, $p = 0.045$), but not time on medication ($p > 0.05$).

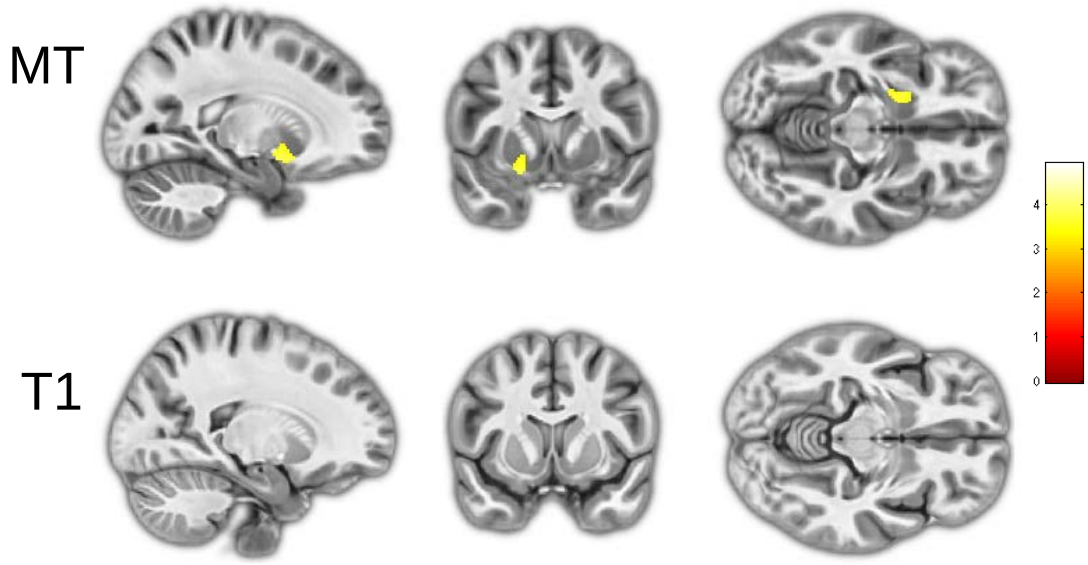

Figure 3.7 Ventral striatal abnormalities in ADHD.

Left ventral striatal volumetric reductions in ADHD detected using MT saturation maps (*p unc.* < 0.001; *FDR* < 0.05) not detected in T1 weighted volumes.

Table 3.1 MT saturation VBM results: ADHD < Controls

Region	Peak Coordinates	Z	*k* *(cluster)*	*p unc.* *(cluster)*	*p (FDR)* *(cluter)*
Left ventral striatum	[-20 9 -14]	3.63	189	0.005	0.043*
	[-18 8 -8]	3.39			
Right inferior parietal	[59 -45 37]	4.46	294	0.001	0.014*
	[51 -42 -28]	4.24			

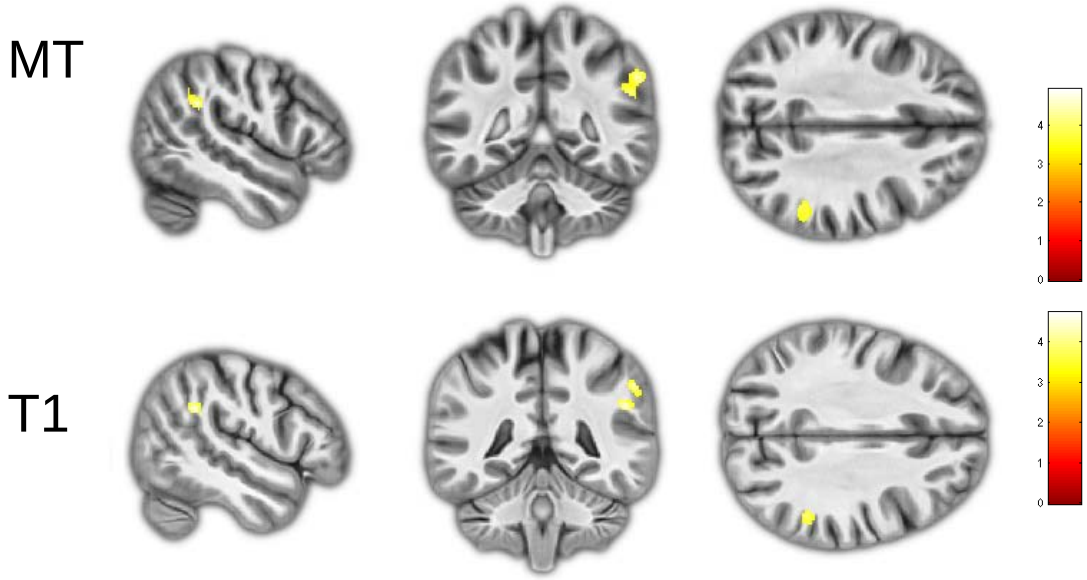

Figure 3.8. Inferior parietal volumetric abnormalities in ADHD.

Left inferior parietal volumetric reductions in ADHD detected using MT saturation maps (*p unc.* < 0.001; *FDR* < 0.05). The same reductions are detected in T1 images (*p < unc. 0.001*) but clusters (*p unc. = 0.027; p unc.* = 0.078) do not survive FDR correction.

Table 3.2 T1 VBM results: ADHD < Controls

Region	Peak Coordinates	Z	*k (cluster)*	*p unc. (cluster)*	*p (FDR) (cluter)*
Right inferior parietal	[51 -43 28]	4.31	111	0.027	0.377
Right inferior parietal	[56 -43 40]	3.87	67	0.078	0.543

3.4 Discussion

Using MT saturation VBM this work reports, contrary to previous findings, that ventral striatal volumetric reductions persist in adults with ADHD even in patients who have undergone long-term treatment with stimulant medication. Moreover, it shows that

identically analysed T1 weighted images of the same subjects are not sufficiently sensitive to detect these striatal abnormalities. Our data therefore strongly suggest that the absence of striatal volumetric differences in previous T1-weighted VBM studies reflect a low methodological sensitivity to subcortical changes, rather than volumetric normalisation associated with maturation or treatment. This appears to arise from poor segmentation accuracy owing to heightened iron content in the striatum. By contrast, both T1 weighted and MT saturation VBM produce similar results in non-subcortical regions such as the inferior parietal cortex.

The observed structural abnormalities in the ventral portion of the striatum indicate the importance of the mesolimbic reward system in ADHD. Inattentive (Volkow et al. 2007) and hyperactive symptoms (Rosa Neto et al. 2002) are linked to striatal dopaminergic signalling, and striatal reward dysfunction (Scheres et al. 2007) is increasingly seen as a central aetiological component of ADHD (Luman et al. 2010). Our findings suggest that these reward system abnormalities persist well into adulthood. This is in contrast to previous meta-analyses which have shifted focus to cortical regions in adulthood, such as the anterior (Frodl & Skokauskas 2012) and posterior cingulate (Nakao et al. 2011). The absence of striatal volumetric reductions in adulthood underpinning this has been suggested to reflect maturational or treatment effects (Nakao et al. 2011). However, this data suggests that this rather reflects difficulties with subcortical segmentation using T1 weighted volumes employed in these studies. Indeed, this work shows that MT saturation VBM has vastly improved sensitivity to striatal abnormalities in adult ADHD when compared to T1 weighted images of the same sample.

Whilst the present findings do not provide support for maturational or treatment related normalisation of the striatum, future longitudinal studies will be needed to directly assess this. Apparent effects of maturation and treatment on striatal volume are certainly credible. However, aging and stimulant treatment may induce various effects on neurobiology that are detectable using MRI aside from grey matter volume. For instance, our data support the association between age (Martin et al. 1998) and ADHD (Cortese et al. 2012; Adisetiyo et al. 2014) (but not medication) with brain iron levels. Future longitudinal work must therefore carefully isolate such factors to accurately study these effects. This is particularly problematic given that one alteration (e.g. brain iron) may interfere with the measurement of another (e.g. volumetric measurement using T1 weighted images) (Helms et al. 2009). Adopting appropriate MR metrics to disentangle these factors and study how they are affected by variables of interest is therefore essential. In particular, this report suggests that T1 weighted imaging of the

striatum is inherently biased by other modulators of the MR signal, and is likely to produce confounded results.

MT saturation maps derived from multi-parameter protocols show greatly enhanced subcortical segmentation, owing to their increased sensitivity to myelin and exclusion of T1-shortening effects of iron (Helms et al. 2009). A variety of measures to index proton density, macromolecular/myelin content and iron can also be derived from such protocols. Such approaches therefore not only enhance sensitivity and specificity of subcortical imaging in ADHD, but also offer a richer range of semi-quantitative indices. Given the inherent problems with T1 weighted imaging of subcortical structures, adoption of multi-parameter sequences into standard imaging protocols would be highly beneficial.

In addition to ventral striatal abnormalities, volumetric reductions within the right inferior parietal lobe are observed. Structural differences within this region has been observed in previous studies though none meeting particularly stringent statistical thresholds (Seidman et al. 2011; N. Makris et al. 2015). However, the direction and laterality of these changes have been inconsistent. For instance, one study has found increased volume in the left inferior parietal lobe (Seidman et al. 2011), whilst one found decreased volume in the left hemisphere and increased volume in the right hemisphere (N. Makris et al. 2015). It is important to note that any directional differences between these previous studies and the present one is not due to the modality used as we detect these changes in analyses of both MT and T1 images. Although the reason for these discrepancies is unclear, these findings all appear to support the importance of attention networks in ADHD. In particular, these reductions appear to be localised within the PFm of the supramarginal gyrus which functionally forms part of the middle inferior parietal lobule (Caspers et al. 2013). The middle inferior parietal lobule (which consists of the PFm and PF subregions) has previously been shown to be activated during nonspatial attention tasks, in particular in re-evaluating conflicting options (Vossel et al. 2006; Boorman et al. 2009; Mevorach et al. 2009; Caspers et al. 2011), as well as spatial attention and reorienting tasks (Rushworth et al. 2001; Corbetta et al. 2008). Interestingly, this region also forms part of the ventral attention network (Corbetta & Shulman 2002) that has been shown to have a role in orienting toward salient stimuli (Fox et al. 2006). Functional connectivity differences in this ventral attention network have also been observed in ADHD (McCarthy et al. 2013) and have been suggested to play a role in distractability in the disorder due to abnormal orienting of attention towards salient stimuli (Aboitiz et al. 2014). Future multimodal (i.e.

structural and resting state functional connectivity) work will be required to assess how these grey matter volumetric abnormalities contribute to dysfunctional ventral attention network connectivity and its neuropsychological consequences.

The present findings encourage interpretative caution in the absence of evidence in T1 weighted imaging studies. This work shows that, rather than reflecting age or treatment related normalisation, the absence of striatal differences in previous studies likely reflects the inadequacy of T1 weighted volumes in detecting them. By contrast, these striatal abnormalities in adult ADHD are readily detectable using MT saturation VBM. Adoption of such protocols offers enhanced subcortical segmentation, and increased statistical sensitivity to detect subcortical abnormalities. Leveraging these benefits is essential in clarifying the role of subcortical structures in ADHD, as both age and disorder related iron content changes may systematically bias analyses using typical T1 weighted images.

4 Microstructure of the mesolimbic and nigrostriatal SN/VTA in ADHD: Relationship to motivation, waiting impulsivity and medication

Theoretical appraisals of Attention Deficit/Hyperactivity Disorder (ADHD) have focussed on aberrant dopaminergic signalling. Whilst the substantia nigra/ventral tegmental area (SN/VTA) is the primary source of dopamine in the brain, little is known of its direct role in the disorder. Recent evidence has strongly implicated reward dysfunction in ADHD, with notable reductions in both incentive motivation and the ability to wait for later rewards, or 'waiting' impulsivity. Preliminary findings have suggested that abnormalities in the SN/VTA may account for these differences in motivational and impulsive profiles. Problematically however, the SN/VTA consists of functionally distinct subcomponents, and previous studies have been unable to localise dysfunction at this sub-structural level. I therefore employ advancements in diffusion MRI tractography to parcellate the SN/VTA, and assess how the microstructure of its mesolimbic and nigrostriatal subcomponents contribute to motivation and waiting impulsivity abnormalities in 30 adults with ADHD when compared to 30 age, IQ, gender and handedness matched controls. Additionally, as psychostimulant medication does not appear to improve waiting impulsivity in animal models of ADHD and actually increases waiting impulsivity in controls, I tested whether this dissociation is also observed in humans in a double-blind placebo controlled manner. This work suggests that increased waiting impulsivity in ADHD is related to FA and MT abnormalities in the mesolimbic SN/VTA. By contrast, no motivational deficits are observed, though this may reflect long-term therapeutic effects of stimulant medication on the nigrostriatal SN/VTA. These results suggest dissociable effects of midbrain dopaminergic subcomponents in ADHD, and a selective effect of long term medication on the nigrostriatal SN/VTA. However, as predicted by animal models, acute stimulant medication had no effect on waiting impulsivity in the ADHD group, and heightened it in controls.

4.1 Introduction

The substantia nigra/ventral tegmental area (SN/VTA) has a central role in dopaminergic modulation of cortico-striatal networks classically associated with ADHD. Even distinct networks prominently implicated in ADHD, such as the default-mode and frontoparietal networks (Konrad & Eickhoff 2010; Castellanos & Proal 2012), appear to show clear dopaminergic modulation by the SN/VTA and its striatal targets (Cole et al. 2013). In spite of this central regulatory role there has been a paucity of work examining the SN/VTA in ADHD, largely due to limitations in non-invasive midbrain imaging.

4.1.1 Abnormal motivation and impulsivity and their relation to SN/VTA subcomponents

Investigations into the neuropsychological mechanisms underpinning ADHD have increasingly come to focus on abnormalities in reward and motivational function that are underpinned by the SN/VTA. For instance, attention problems in the disorder may reflect abnormalities in incentive motivation (Volkow et al. 2011). Similarly, hyperactive/impulsive symptoms in the disorder may be related to a more specific form of 'waiting' impulsivity, most frequently characterised by increased temporal discounting of reward values (Thorell 2007; Scheres et al. 2008; Scheres et al. 2010).

Preliminary work has suggested that both motivational abnormalities in ADHD (Volkow et al. 2011) and trait impulsivity (Buckholtz et al. 2010) are linked to SN/VTA D2/D3 receptor binding. However, the SN/VTA is not a functionally homogenous structure, and previous findings have been unable to determine whether these abnormalities are specific to a particular SN/VTA subregion. This is essential, as these subcomponents are characterised not just by distinct functional roles and anatomical connectivity (Haber et al. 2000; Haber 2003; Haber & Knutson 2010), but also remarkably different pharmacological response profiles (Browder et al. 1981; Ashby et al. 2000; Gervais & Rouillard 2000; Mereu et al. 1987; Klink et al. 2001; Mejías-Aponte et al. 2009; Goldstein & Litwin 1988). This work therefore uses diffusion MRI tractography to parcellate the SN/VTA into these functional subcomponents.

4.1.2 Background to diffusion MRI tractography based parcellation

4.1.2.1 Diffusion MRI

Diffusion is the random translational motion of molecules resulting from their thermal energy. Hydrogen protons within water molecules that form the basis of most biological MR applications are subject to this process, obeying a Gaussian distribution within a free medium. The biologically informative nature of diffusion MRI rests on the sensitivity to detect and quantify such diffusion processes, and how they are moderated by their surroundings.

In biological tissues, diffusion MRI is sensitive to the hindrance of diffusion by tissue microstructure (Le Bihan 2003), and thus provides an indirect measure of the size, orientation, and shape of cellular structures in vivo. Diffusion MR exploits the natural sensitivity of MRI to motion, using a pair of gradient pulses. The first results in excitation of protons that varies according to their spatial location. A second pulse is then used to detect changes in displacement since the first. This approach to measuring diffusion enables the diffusion coefficient to be measured along a single direction at a time. Very early on it became clear that in the white matter of the brain the diffusion coefficient strongly depends on the direction of measurement. At the microstructural level, highly myelinated axons greatly hinder diffusion in directions perpendicular to the axon, but allow for largely unrestricted diffusion along these axonal pathways (Moseley et al. 1990). This property is termed diffusion anisotropy. In analogy with other anisotropic phenomena, diffusion can be described by a 3x3 tensor matrix (Basser et al. 1994), which enables the overall tissue directionality within a voxel to be characterized. The elements of the tensor are defined with respect to a specific frame of reference, and thus are different for each system of coordinates; however, it is possible to define a number of scalar quantities that are rotationally invariant. The most popular are the mean diffusivity (MD), which reflects the magnitude of diffusion, irrespectively of directionality, and the fractional anisotropy (FA; (Basser & Pierpaoli 1996)), which quantifies the directionality of the tensor in a voxel. As the diffusion tensor is symmetric and positive definite, it has 6 unique elements. It is therefore possible to estimate its components by collecting a minimum of 6 images, weighted along 6 non-collinear directions, and a non-diffusion weighted scan. Multivariate linear regression can then be performed based on the tensor model. This procedure also

allows the principal direction of diffusion in a voxel to be derived. In practice, due to the presence of noise, a much larger number of images are acquired.

4.1.2.2 Higher order models

While characterizing diffusion using a tensor allows anisotropy and principal direction of diffusion to be obtained, the model is unable to resolve complex intra-voxel structures such as crossing or branching fibers. More complex models, aiming at deriving directional information from the molecular displacement profile have been introduced. This work employs one of these models, persistent angular structure (PAS) MRI (Jansons & Alexander 2003), which samples the Fourier transform of the probability density function of the water molecular displacements.

4.1.2.3 Tractography

Based on the assumption that the principal direction of diffusion in a voxel coincides with the principal axonal direction, patterns of contiguous inter-voxel directionality have offered a method for constructing representations of white matter pathways within the brain (Basser & Pierpaoli 1996; Mori et al. 1999; Basser et al. 2000; Catani et al. 2002). This method of tractography has been shown to produce 'reconstructions' of white matter pathways that offer a reasonable representation of anatomy determined by more accurate but invasive *ex-vivo* methods such as post-mortem blunt dissections and axonal tracing studies (Lawes et al. 2008). There are two main types of tractography algorithms: deterministic and probabilistic. Deterministic tractography follows the principal direction of diffusion to reconstruct estimates of the path of fibre bundles. This algorithm produces a single trajectory, often described as a streamline. The probabilistic approach considers multiple pathways emanating from a single seed-point, and assigns a probability of connection to the seed-point to every voxel in the brain. This chapter focusses specifically on the application of such probabilistic tractography methods to parcellate grey matter into functional subregions according to their anatomical connectivity.

4.1.2.4 Diffusion tractography based parcellation

Tractography based parcellation of grey matter is motivated by the concept that the functional specialization of grey matter is in large part defined by its patterns of connectivity to other brain regions. Exploiting this has been a central component to understanding regional specification beyond the capacity of traditional structural

imaging techniques, as functional specialization does not necessarily obey the traditional anatomical boundaries of nuclei and laminal surfaces, and gyri and sulci. An example of particular interest is the functionally defined ventral striatum. Whilst this is largely taken to correspond to the nucleus accumbens, this also encompasses surrounding medial and ventral putamen and caudate regions (Haber 2003). Due to this lack of confinement to typical anatomical boundaries, the extent of ventral striatum is not delineable using traditional structural imaging alone. Instead, the ventral striatum can be defined by its different patterns of connectivity to, amongst other regions, more medial and ventral regions of frontal cortex than the dorsal component of the striatum, which preferentially connects to more dorsal and lateral frontal regions (Haber 2003). Tractography based parcellation can therefore use these different patterns of connectivity to define functionally distinct ventral and dorsal subregions within the striatum.

The first application of this approach focused on the nuclei of the thalamus (Behrens et al. 2003). These thalamic subregions, due to their connections to distinct cortical regions, control the relay of information necessary for a range of different function. The parcellation required the definition of a seed-region to be segmented (in this case the thalamus) and a set of target regions, known to be connected to the seed (in this case, separate cortical regions). By performing probabilistic tractography for each voxel corresponding to the thalamus in a diffusion dataset, produced probability of connection to each of the targets can be assigned to it. In this early example, this allowed estimation of the most densely connected cortical target region for each thalamic voxel using a winner-takes all strategy (Behrens et al. 2003). Similar techniques have been applied to the SN/VTA.

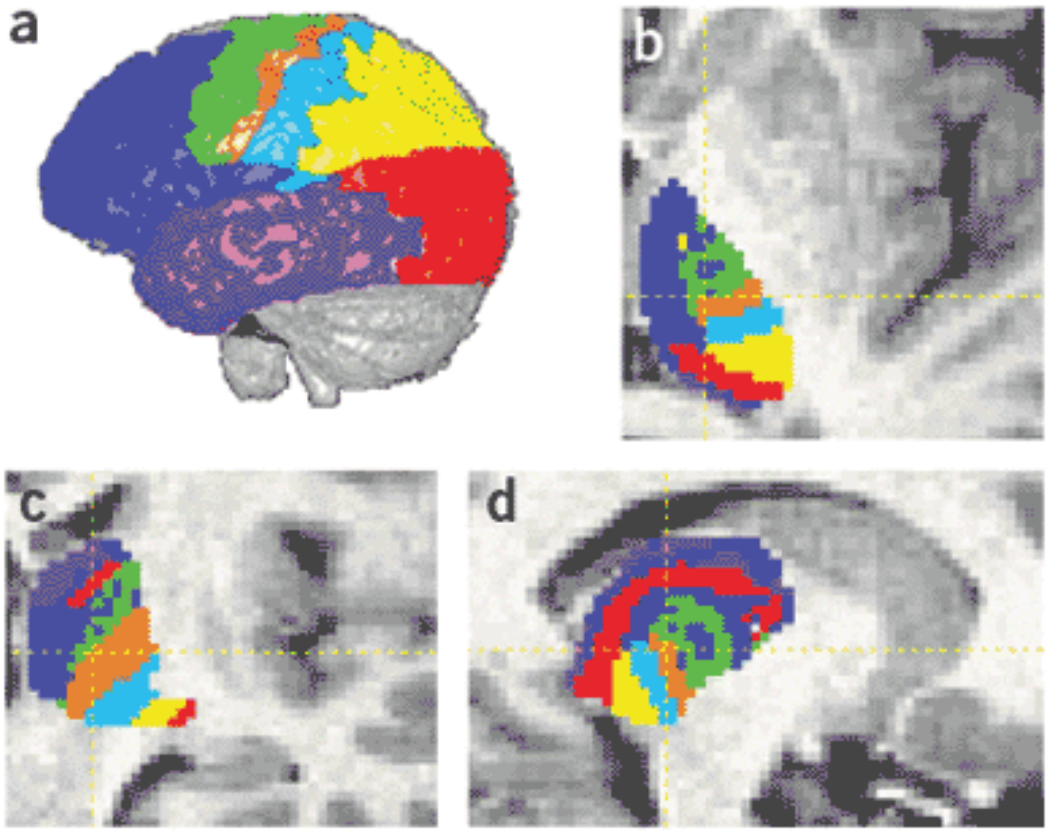

Figure 4.1 Parcellation of the thalamus according to cortical connectivity.

Seven cortical target ROIs, and a thalamic target region are defined. After this, 10,000 streamline iterations were produced for each thalamic seed voxel, with the probability of connectivity to each target determined as the number of streamlines connecting the seed to that target. Seed identity was then determined according to a winner-takes-all strategy (ie each seed region is defined by the target with the greatest connection probability.

Adapted from (Behrens et al. 2003)

4.1.2.5 Parcellation approaches to the SN/VTA

Although MT saturation maps offer vastly improved SN/VTA contrast, the subcomponents of the SN/VTA appear as a single continuous hypo-intense region with no discriminable boundaries. Two previous studies have however successfully exploited the differential connectivity patterns of these subcomponents to parcellate the SN/VTA into functional subdivisions (Menke et al. 2010; Chowdhury et al. 2013). One approach using a target ROI, winner-takes-all method as the above example, used the preferential connectivity of the mesolimbic/dorsomedial SN/VTA and the nigrostriatal/ventrolateral SN/VTA to the ventral and dorsal striatum respectively (Chowdhury et al. 2013). The second paper adopted an alternative approach, using k means clustering to parcellate the SN into the SNpc and SNpr respectively without prior target regions (Menke et al. 2010). As the focus of this chapter is the dopaminergic midbrain specifically, and since we can rely on strong prior anatomical hypotheses regarding these connections due to previous animal work (Haber 2003; Haber & Knutson 2010), this work employ an adaptation of the first approach.

4.1.3 Parcellation of the mesolimbic and nigrostriatal SN/VTA

This approach also allows assessment of prior hypotheses about the neural correlates of motivation and waiting impulsivity. Waiting impulsivity in particular is partially underpinned by dopaminergic processing within the nucleus accumbens (Economidou et al. 2012). It would therefore be expected that the mesolimbic, rather than the nigrostriatal, SN/VTA would be responsible for this dopaminergic modulation. However, no work to date has assessed this. The correlates of incentive motivation within the SN/VTA also remain unclear. As noted previously, whilst early accounts suggested that the mesolimbic SN/VTA and ventral striatum underpin incentive motivation, converging evidence suggests that the SNpc (Rossi et al. 2013) and dorsal striatum (Volkow et al. 2002; Tomer et al. 2008). may be responsible for motivational processing. This work therefore employs this mesolimbic/nigrostriatal distinction to assess how abnormalities in waiting impulsivity, as indexed by a recently developed human 4-choice serial reaction time (4CSRT) task (Voon et al. 2014; Voon et al. 2015) (based on the animal 5CSRT task (Robinson et al. 2009)) and trait motivation are

localised in the SN/VTA in ADHD. In doing so, this also offers three advancements to the techniques used in the prior study.

Firstly, I expanded the connectivity target regions to other important subcortical structures that are preferentially connected the mesolimbic SN/VTA – namely the amygdala and hippocampus (Haber & Knutson 2010). Secondly, due to the small size of the SN/VTA, a novel upsampling method which is detailed below was applied to the diffusion data to perform the analysis at a higher resolution. Finally, rather than using a tensor (ie DTI) model that computes only one principal direction (PD) of diffusion, PAS MRI was employed (Jansons & Alexander 2003), modelling diffusion in up to three PDs per voxel. In addition to resolving crossing fibre configurations, this allows more accurate modelling of potentially multidirectional projections from a single seed voxel.

4.1.4 Extending the concept of waiting impulsivity in adult ADHD: 'Premature responding' and acute effects of medication

As noted, most work examining waiting impulsivity in ADHD has focused on TD. By contrast, a rich literature has also developed in animal models examining 'premature responding' to reward cues using the 5CSRT (Dalley et al. 2011). The 5CSRT has recently been translated to humans (Voon et al. 2014), which also offers the possibility of confirming several pharmacological findings in animal models. Specifically, work with animal models of ADHD suggest that poorer performers do not benefit from stimulant treatment on the rodent 5CSRT (Paterson et al. 2011), whilst normal performers actually see increased waiting impulsivity (Navarra et al. 2008). As an additional component to this work, I therefore also sought to assess the differential role of stimulant medication on waiting impulsivity (measured by the 4CSRT) in ADHD and the healthy population.

4.2 Methods

4.2.1 Participants

The same cohort of thirty patients with ADHD (mean 34 (±9.5) years; 19 male) and 30 healthy control participants (mean 33 (± 9.5) years; 19 male) described previously were included in the study.

4.2.2 Questionnaires

The Conner's self-report Adult ADHD Rating Scale (CAARS)(Conners et al. 1999) was used to index current ADHD symptom severity, and Beck's Depression Inventory (BDI; (Beck et al. 1996)) and the State and Trait Anxiety Inventory (STAI;(Spielberger 1983)) were used to assess depression and anxiety scores respectively. The Tridimensional Personality Questionnaire (TPQ; (Cloninger et al. 1991)) and Multidimensional Personality Questionnaire (MPQ) were administered (Tellegen & Waller 2008), with their respective persistence and achievement (as in (Tomer et al. 2008; Volkow et al. 2011)) subscales used as measures of trait motivation.

4.2.3 Waiting Impulsivity Task

Waiting impulsivity was measured using a computerised 4C-SRT task for humans (Voon et al. 2014). Participants were seated in front of a touch screen monitor. When four boxes appeared on the screen, the subject pressed and held down the space bar on the keyboard with their dominant index finger, indicating the 'cue onset' time. After a specified period (cue-target interval), a green circle appeared briefly and randomly in one of the four boxes. Subjects were previously instructed to release the space bar upon this cue, and touch the on-screen box in which the target had appeared (Figure 4.2). Fast and accurate responses were rewarded, with faster accurate responses rewarded more highly than slower ones (Figure 4.2). The primary outcome measures for impulsivity were premature responses (ie presses before the reward cue) and premature releases and responses combined (ie releases of the space bar before the reward cue, including both premature responses and when no response was made). These measures thus indexed impulsive waiting for reward, defined operationally as the tendency to respond *before* the onset of a reward cue (Robbins 2002). This

therefore reflects a form of an inappropriate anticipatory response to expected but uncued reward.

Two baseline blocks without monetary feedback were used to individualize monetary feedback amounts for subsequent blocks on the basis of the mean fastest reaction time (RT) and SD of the individual. Four Test blocks with monetary feedback were optimized to increase premature responding and varied by duration and variability of the cue-target interval and the presence of distractors. The block order for the task was as follows: Baseline block 1; Test block 1; Baseline block 2; Test blocks 2–4. Twenty-five participants with ADHD, and 28 controls completed the task.

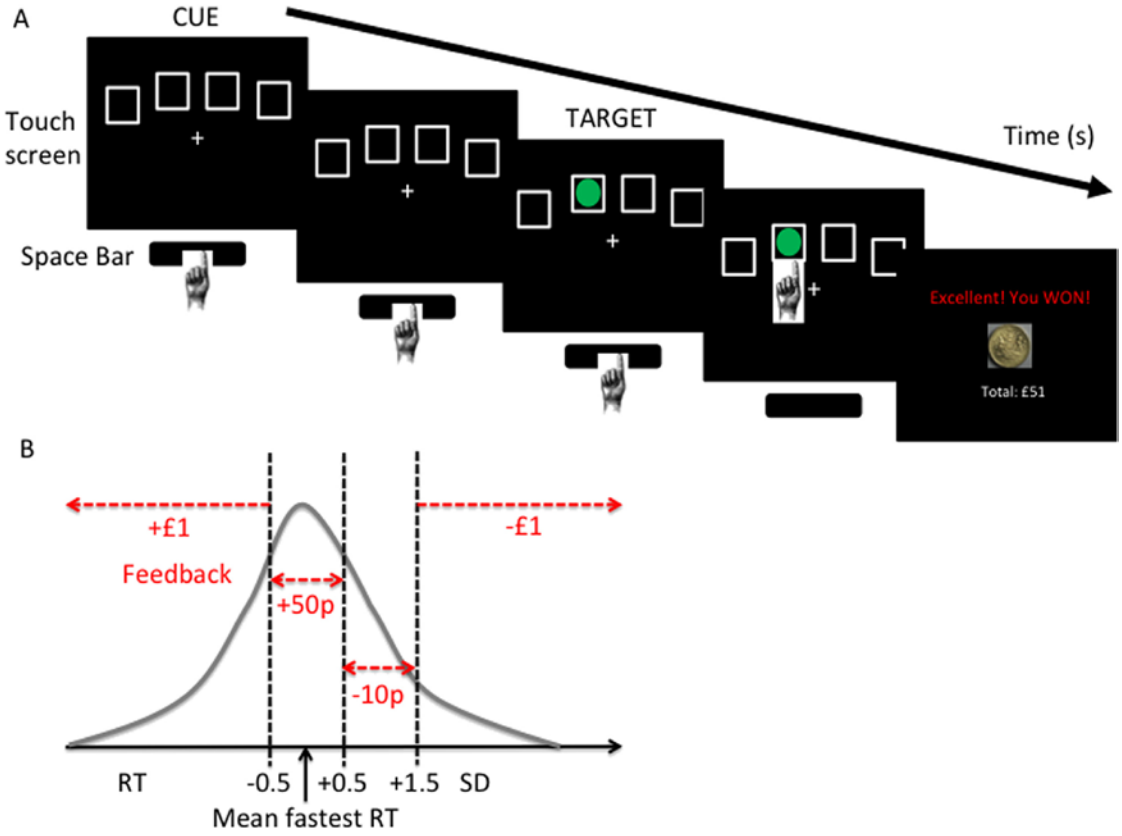

Figure 4.2 Outline of 4-CSRT task.

A) Representation of 4-CSRT task. Participants were instructed to hold their finger on the space bar until a green dot appeared, at which point why removed their finger to tap the location of the green dot. B) Participants were given reward feedback, with rewards contingent on accurate responses and the amount won or lost determined by response speed.

4.2.4 Procedure

ADHD and healthy controls underwent scanning and behavioural testing as part of the double-blind placebo-controlled study previously detailed. After scanning and behavioural tests previously reported, participants underwent the 4C-SRT approximately 3 hours after ingestion of drug or placebo. See Chapter 2 for further details on timing of procedures.

4.2.5 MRI

All scanning was performed on a 1.5T Siemens Avanto. The scanner's body coil is used for RF transmission, and a 32-channel head coil for signal reception. For diffusion MR imaging a multi-slice twice refocused spin echo echo-planar imaging (EPI) acquisition was used, with 60 contiguous near axial slices acquired with 2.5mm^3 isotropic voxels. Acquisition had a TE of 86ms, and a TR of 7.7s. A maximum diffusion weighting of b=1500 smm^{-2} was applied. 60 diffusion-weighted brain volumes with diffusion gradients uniformly distributed in space were collected at each slice location, as well as 7 volumes without diffusion weighting applied.

MT maps were calculated from a multi-parameter protocol adapted from a 3D multi-echo fast low angle shot (FLASH) sequence, described in chapter xx.

4.2.6 ROI definition

SN/VTA seed regions were traced, blind to diagnosis, on MT saturation maps. Freesurfer's *recon_all* function was used to derive subject specific masks for target ROIs (Fischl et al. 2002). For the nigrostriatal target, the caudate and putamen were combined into a dorsal striatal ROI. For the mesolimbic target, I extended previous work (Chowdhury et al. 2013) which had defined the mesolimbic portion of the SN/VTA by its connectivity to the nucleus accumbens alone. Due to the additional, well-defined mesolimbic connectivity patterns with the amygdala and hippocampus (Haber 2003; Haber & Knutson 2010), these regions were also included in the mesolimbic target. Freesurfer segmentation quality was carefully inspected before use. Data from one

participant, for whom a reliable segmentation could not be gained, was excluded from tractography analyses.

4.2.7 Preprocessing

Diffusion weighted (DW) volumes were corrected for eddy currents distortions and involuntary motion by affine registration. First, a within b-value coregistration was performed, and average b=0, and b=1500 smm^{-2} images were created and skull-stripped. The average DW image was coregistered to the mean b=0 image to obtain the transformation matching them. Each DW volume was realigned to the mean DW image and the transformation matching each DW volume with the b=0 image was obtained by combining the partial transformations from either previous steps. B matrices were then rotated according this combined transformation (Leemans & Jones 2009). The diffusion tensor was then estimated in every voxel and FA maps were exported using Camino (Cook et al. 2006). A PAS model of diffusion (Jansons & Alexander 2003) was then fitted at every voxel to obtain the fibre orientation distribution (FOD). The local maxima of this function corresponding to the principal directions of diffusion (PDs) were then extracted for each voxel, with a maximum of three PDs extracted per voxel.

Due to the small size of the SN/VTA connectivity-based parcellation was performed at the higher spatial resolution of the MT data, rather than the native diffusion space. Due to the nature of diffusion data, this operation requires a more complex pipeline than a simple coregistration. First, FA maps for each subject were warped to MT saturation maps using an initial affine transformation (T_{aff}) and a diffeomorphic non-linear transformation (T_{diff}) (using a greedy symmetric normalisation SyN model; (Avants et al. 2011)). To simplify rotation of the PDs in the transformation of diffusion data I applied only the linear (T_{aff}) transform to the diffusion data, and used the inverse non-linear (T_{diff}) transform to warp ROIs into this intermediate 'affine' space (Figure 4.3). As PDs from the PAS function are represented by vectors, a dyadic tensor was calculated from each set of PDs to preserve directional information during transformation as in (Cercignani et al. 2012). Diffusion data were therefore transformed according to T_{aff} with dyadic tensors rotated accordingly, before deriving new PDs from the tensors. Finally, probabilistic index of connectivity (PiCo) maps were then calculated for probabilistic tractography.

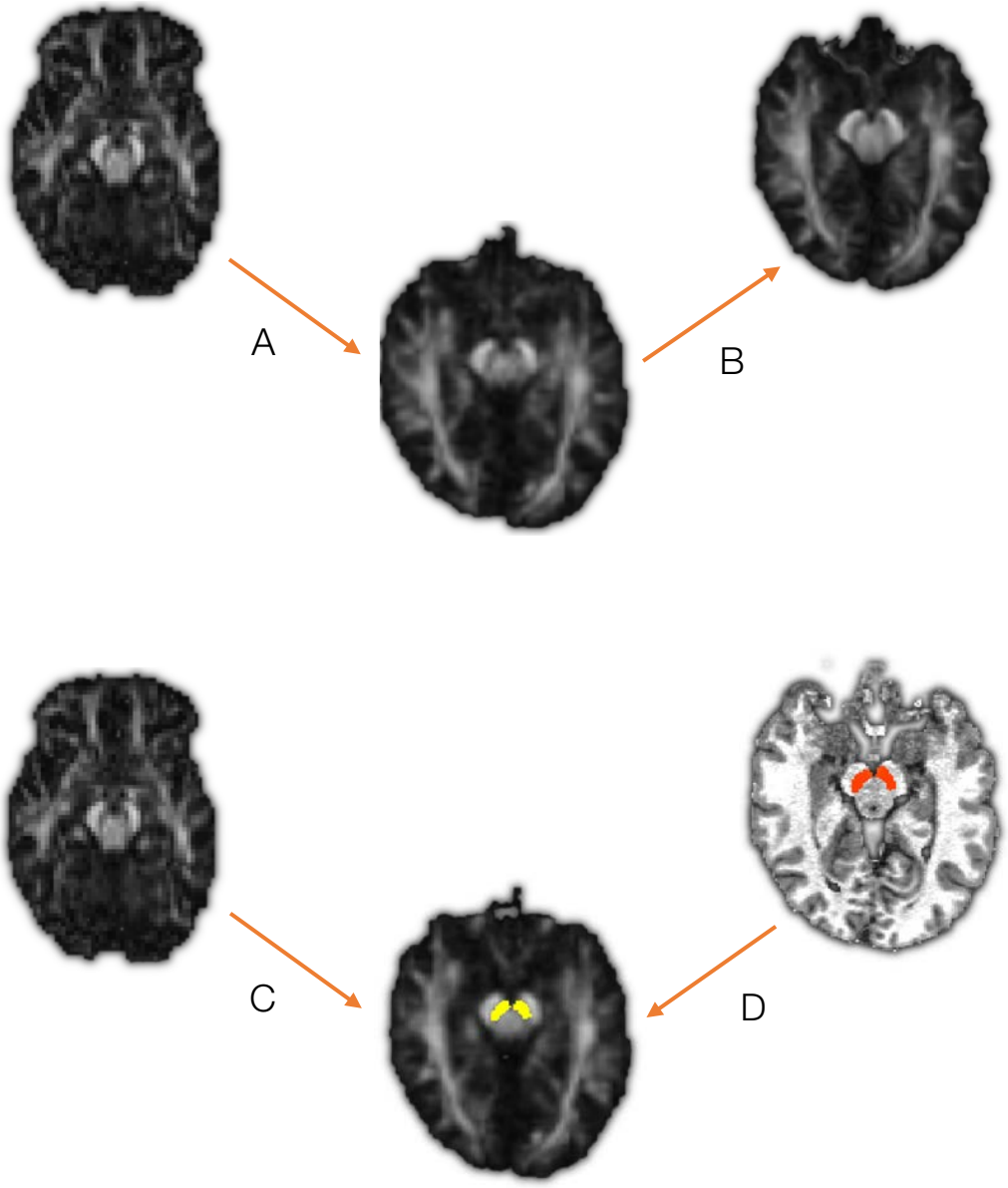

Figure 4.3 Co-registration pipeline for tractography analysis

FA images were registered to MT saturation maps with A) an initial affine transformation followed by B) a diffeomorphic nonlinear registration. Diffusion information were C) registered to intermediate 'affine' space (using transformation A) to simplify rotation of PDs. For this transformation, PDs were transformed into dyadic tensors to preserve rotational information, before being converted back to PDs. D) ROIs were transformed from MT space using the inverse diffeomorphic transform (from B).

4.2.8 Diffusion MRI tractography

Probabilistic tractography was performed using Euler integration and linear interpolation, and 5000 iterations for each PD in each seed voxel. Streamlines terminated when they reached either the dorsal striatum or limbic targets, or if they exceeded a curvature threshold of >80°. Each voxel connectivity value was then used to binarise the connection probability maps for each seed with a winner-takes-all strategy across each of the PDs. For group average map visualisation, results were transformed into a common space and thresholded at 50% of their maximum overlap.

4.2.9 Extraction of mean ROI microstructural indices

Micostructural indices were extracted from MT saturation and FA maps using subject-specific binarised masks of the nigrostriatal and mesolimbic SN/VTA produced during the tractography analyses.

4.2.10 Statistics

Statistical analyses were performed in SPSS 22. Repeated measures mixed model ANOVAs used to assess group differences in FA and MT separately, with Hemisphere and Subcomponent as within subject factors. Correlations were calculated Pearson's *r* partial correlation. Data were assessed for normality and normalised where possible, with medication duration log-transformed. In cases where transformations did not yield a normal distribution (TPQ 'Persistence' and MPQ 'Achievement' subscales), Spearman's *rho* partial correlations were used instead. One extreme outlier (> 4 SD from mean) in the 4CSRT RT data was removed. All comparisons were controlled for age, and BDI and trait anxiety scores, with additional control for total intracranial volume for brain imaging data.

4.3 Results

4.3.1 Behavioural findings

4.3.1.1 Premature responding

A significant drug*group interaction was observed for premature releases and responses ($F_{(1,48)}$ = 4.13, p = 0.048). Post hoc tests revealed that on placebo, the ADHD group were more prone to premature releasing and responding (17.4 ± 11.2) than the control group (12.1 ± 8.9) at trendwise significance (p = 0.063). Interestingly, drug administration showed a trend towards increased premature releases and responses in the control (20.3 ± 27.7; $F_{(1,27)}$ = 3.09, p = 0.090), but not the ADHD group (17.4 ± 11.7; $F_{(1,27)}$ = <0.01, p = 0.990). A similar interaction was also observed for premature releases/responses alone ($F_{(1,48)}$ = 4.12, p = 0.048), with the ADHD group showing similar performance on drug (9.9 ± 7.1) and placebo (8.4 ± 6.6), and increased premature responding/releasing in the control group on drug (9.4 ± 19.8) compared to placebo (6.5 ± 5.2). However, post-hoc testing did not reveal any trends towards significance between the ADHD and control groups on premature releasing alone. No differences in reaction time were observed (Group x Drug: $F_{(1,47)}$ = <0.01, p = 0.957; Drug: $F_{(1,47)}$ = 0.31, p = 0.578; Group: $F_{(1,47)}$ = <0.01, p = 0.957 (Table 4.1).

Table 4.1 Behavioural responses on 4CSRT task

Measure	Mean scores (SD)	
	ADHD	Controls
Drug		
Prem. responses	9.9 (7.1)	9.4 (19.8)
Prem. releases & responses	17.4 (11.7)	20.3 (27.7)
Reaction time (ms)	605.0 (263.3)	609.1 (126.9)
Placebo		
Prem. responses	8.4 (6.6)	6.5 (5.2)
Prem. releases & responses	17.4 (11.2)	12.1 (8.9)
Reaction time (ms)	578.7 (135.4)	593.0 (105.5)

4.3.1.2 Motivation

In contrast with previous results in medication-naïve subjects with ADHD (Volkow et al. 2011), there appear to be no differences in motivation compared to controls in either the TPQ (ADHD: 5.3 ± 2.3; Control: 4.7 ± 2.0; $F_{(1,54)} = 0.77$, $p = 0.383$) or MPQ subscales (ADHD: 11.8 ± 5.1; Control: 11.4 ± 4.5; $F_{(1,54)} = 2.45$, $p = 0.123$).

4.3.2 Parcellation

The parcellation produced results comparable with animal tracer studies (Haber et al. 2000) and previously published parcellations of the substantia nigra (Chowdhury et al. 2013). This reveals a nigrostriatal cluster (Left: 533.7±161.95mm^3 Right: 548.7±135.40161.95mm^3) comprising the ventrolateral portion of the SN/VTA, and a mesolimbic cluster (Left: 103.2±68.58mm^3 Right: 90.0±62.20mm^3) in a more dorsomedial region (Figure 4.4).

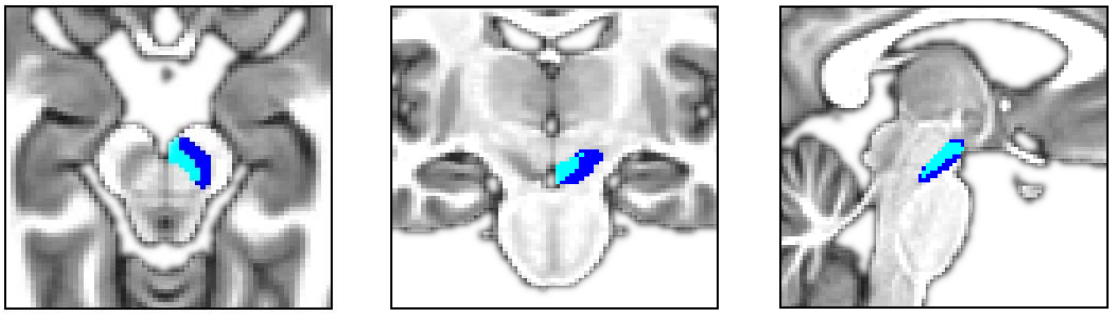

Figure 4.4 Parcellation of the SN/VTA into mesolimbic (light blue) and nigrostriatal (dark blue) components.

Table 4.2. Fractional anisotropy and MT saturation values in the SN/VTA

Measure	Mean scores (SD)		F	p
	ADHD	Controls		
FA				
L. Nigrostriatal	0.411 (0.030)	0.415 (0.029)	1.00	0.323
L. Mesolimbic	0.339 (0.048)	0.366 (0.047)	4.98	0.030*
R. Nigrostriatal	0.413 (0.031)	0.423 (0.027)	2.90	0.094
R. Mesolimbic	0.338 (0.065)	0.340 (0.042)	0.02	0.897
MT				
L. Nigrostriatal	4.563 (0.210)	4.561 (0.564)	0.41	0.526
L. Mesolimbic	3.810 (0.564)	4.110 (0.431)	3.84	0.055
R. Nigrostriatal	4.591 (0.222)	4.602 (0.212)	1.35	0.251
R. Mesolimbic	3.857 (0.823)	3.713 (0.575)	0.45	0.503

4.3.2.1 Substantia nigra/ventral tegmental area microstructural measures

Differences were observed in FA of SN/VTA subregions, with a significant group x subregion x hemisphere interaction ($F_{(1,54)}$ = 4.39, p = 0.041), with post hoc comparisons revealed significant differences in the left dorsomedial component (p = 0.030), and trend to significance in the right ventrolateral component (p = 0.094; Table 4.1). Group differences in MT saturation in these regions were also observed (group x subregion x hemisphere; $F_{(1,54)}$ = 4.20, p = 0.046).

4.3.2.2 Relationship between behavioural measures and SN/VTA microstructure

Increased waiting impulsivity in ADHD was associated with reduced FA (Responses: r = -0.59, p = 0.006; Responses and Releases: r = -0.55, p = 0.012) and MT saturation level (Responses: r = -0.48, p = 0.032; Responses and Releases: r = -0.49, p = 0.028) in the right mesolimbic SN/VTA. By contrast, both greater trait motivation in patients (MPQ: *rho* = -0.50, p = 0.014; TPQ: *rho* = -0.39, p = 0.066) were selectively related to FA within the right nigrostriatal SN/VTA. Interestingly, the length of time (r = -0.47, p = 0.020) for which patients had been medicated was also related to FA in the right nigrostriatal SN/VTA, suggesting long term effects of medication on the SN/VTA subregions underpinning incentive motivation.

4.4 Discussion

Failure to inhibit premature responses during waiting is a central component to theoretical conceptualisations of impulsivity in ADHD. Similarly, motivational abnormalities have become an increasingly salient marker of dopamine system dysfunction in the disorder. This work shows an anatomical dissociation of these two abnormalities at the level of the dopaminergic midbrain: Whilst disruptions to the mesolimbic SN/VTA appear to contribute to waiting impulsivity in ADHD, trait motivation appears to be linked to the nigrostriatal component. However, in contrast to previous findings in medication naïve patients (Volkow et al. 2011), trait motivation is not reduced in those have been treated with stimulant medication. Instead, this data suggests that long term stimulant treatment of ADHD is associated with microstructural changes consonant with increased motivation in the disorder.

In order to accurately separate the mesolimbic and nigrostriatal components of the SN/VTA this work used their connectivity patterns, as defined by DWI tractography. While this had been achieved before (Chowdhury et al. 2013), here I introduced a number of methodological improvements. First, instead of DTI, a PAS model of diffusion was used, allowing for up to 3 PDs per voxel. In addition to resolving crossed fibre configurations during tractography, this also better models potentially multidirectional projections from seed regions enhancing intra-voxel parcellation accuracy. Next, tractography was performed in the higher resolution space of the MT images, thus obtaining finer parcellation of the SN/VTA and reducing the variance associated with winner-takes all approaches to seed voxel classification. Finally, this work incorporates further classifier regions that are known to connect to the mesolimbic SN/VTA to improve parcellation accuracy.

We report that heightened waiting impulsivity in ADHD is linked to a disruption of anisotropic tissue organization in the mesolimbic SN/VTA. Consonant with blunted mesolimbic dopaminergic systems in ADHD (Volkow et al. 2007; Volkow et al. 2011; Silvetti et al. 2013), this pattern of reduced FA (Vaillancourt et al. 2009) and MT measures (Eckert et al. 2004) has been linked to dopaminergic midbrain degeneration in Parkinson disease.

Whilst numerous mechanisms including reward valuation and cognitive control have been shown to contribute to temporal discounting (Peters & Büchel 2011), our data suggest that waiting abnormalities in ADHD appear to be at least in part underpinned by disruption to the midbrain reward system. Further specification of the mechanisms underpinning this is required, however. Abnormal valuation of temporally distant rewards has frequently been suggested to underpin waiting deficits in ADHD (Luman et al. 2005; Sonuga-Barke et al. 2008). However, as the mesolimbic SN/VTA also has a prominent role in aversion (Lammel et al. 2012), and our results may also reflect an abnormal aversive valuation of waiting. Future work will be required to discern to what extent these two mesolimbic processes contribute to waiting impulsivity.

Our findings that methylphenidate did not ameliorate waiting impulsivity in ADHD mirror findings in animal models (Paterson et al. 2011) and suggest that a review of pharmacological therapies used to treat impulsivity may be required. This lack of efficacy may well reflect the promiscuity of methylphenidate at both dopamine and noradrenaline transporters, as these catecholamines have opposing waiting impulsivity-enhancing and -reducing effects respectively in the nucleus accumbens

core and shell (Economidou et al. 2012). Contrastingly, by selectively targeting blockade of the noradrenergic transporter atomoxetine has shown far more promise in treating waiting impulsivity in animals models (Navarra et al. 2008; Paterson et al. 2011; Economidou et al. 2012; Parker et al. 2014). Whilst translation of these effects to humans is necessary before definitive recommendations can be made, this may have far-reaching clinical implications for how different subtypes of ADHD should be pharmacologically targeted.

These findings also have implications for use of methylphenidate as a cognitively-enhancing agent in the healthy population (Sahakian & Morein-Zamir 2015). In line with previous observations in humans (Voon et al. 2015) and rodents (Navarra et al. 2008; Loos et al. 2010) these data show that healthy, non-impulsive subjects show increases in waiting impulsivity when given methylphenidate. These findings add to a growing body of evidence that whilst methylphenidate confers some similar cognitive gains in healthy individuals and controls (Agay et al. 2010), there is a clear divergence of effects in other functions. Interestingly, this divergence seems to be most profound in behaviours and functions typically associated with 'core' dopaminergic processes, such as reinforcement learning (See Chapter 5) and impulsivity. Given these striking differences in acute effects, it is worthy of concern that the long term safety and tolerability of methylphenidate use that is observed in ADHD may not be transferable to the general population.

In line with findings that have shifted research into incentive motivation to the SNpc (Rossi et al. 2013) and more dorsal aspects of the striatum (Volkow et al. 2002; Tomer et al. 2008), this work shows that motivation appears to be linked to the nigrostriatal SN/VTA. Our findings combined with these previous results suggest a role of the nigrostriatal SN/VTA and its afferent dorsal striatal regions as opposed to mesolimbic SN/VTA and the ventral striatum. However, unlike stimulant naïve participants (Volkow et al. 2011), patients who have been medicated long term do not appear to present with reduced motivation. Our data suggest that this may reflect therapeutic effects of long term medication on the nigrostriatal SN/VTA that are consonant with heightened motivation.

Methylphenidate acutely enhances motivation in ADHD (Chelonis et al. 2011), and normalizes activity in motivational networks (Rubia et al. 2009). Methylphenidate enhancement of D2/D3 receptor signaling in motivational regions such as the ventral striatum also predict improvements in attention after long term treatment with

methylphenidate (Volkow et al. 2012). Similar to reports of structural grey matter changes in response to treatment in ADHD (Frodl & Skokauskas 2012), our findings are suggestive of long term microstructural alterations in the nigrostriatal SN/VTA.

One possible explanation for the relationship between longer periods of medication and motivation with lower diffusion anisotropy in the nigrostriatal SN/VTA may be explained by downstream effects on cell morphology and organization that enhance intraregional communication. Methylphenidate-driven upregulation of BDNF and GDNF (Roeding et al. 2014; Simchon-Tenenbaum et al. 2015) can induce such neurotrophic and protective changes in the SN/VTA (Lin et al. 1993; Tomac et al. 1995; Hyman et al. 1991) and GDNF in particular has been shown to increase axonal sprouting and cell survival but not striatal innervation by midbrain neurons (Rosenblad et al. 2000). Accordingly, reduced FA that is observed in long term treatment could reflect local, multidirectional neurite growth. Such an explanation would therefore posit that methylphenidate upregulates various growth factors that increase multidirectional neurite growth in the nigrostriatal SN/VTA which consequently improves motivation.

Although such an explanation remains speculative, GDNF and BDNF plasma levels are abnormal in ADHD (Shim et al. 2015; Corominas-Roso et al. 2013; Shim et al. 2008) and are altered by stimulant medication (Amiri et al. 2013). Further molecular studies will be required to elucidate the therapeutic role of these molecules in long term stimulant treatment, if any. Similarly, future work using models of diffusion that can assess neurite dispersion and density accurately in grey matter may offer direct measures of the multidirectional neurite growth posited here to explain reduced FA (Zhang et al. 2012). Although the mechanisms of these changes is highly speculative, it is noteworthy that the directionality within these regions is supported by another study. Specifically, patients with depression who are associated with reduced motivation, show *heightened* FA in the SN/VTA (Blood et al. 2010). This is consonant with our findings that indicate that increased motivation is somewhat counter-intuitively linked to *reduced* FA.

Further research examining the acute and longitudinal effects of medication is also necessary. This work specifically studied trait motivation, adopting measures used in previous medication naïve studies (Volkow et al. 2011). Although using standardized metrics has the appeal of replicability and comparison between studies, such measures are not appropriate for measuring acute effects of medication. Future work modelling different components of motivation (Berridge 2012) will be essential to better